Title

EPH/EPHRIN regulates cellular organization by actomyosin contractility effects on cell contacts

Journal

Journal of Cell Biology, 220(6)

ISSN

0021-9525

Authors

Kindberg, Abigail A
Srivastava, Vasudha
Muncie, Jonathon M
et al.

Publication Date

2021-06-07

DOI

10.1083/jcb.202005216

Peer reviewed

JCB Journal of Cell Biology

ARTICLE

EPH/EPHRIN regulates cellular organization by actomyosin contractility effects on cell contacts

Abigail A. Kindberg[1,2,3,4,5], Vasudha Srivastava[6], Jonathon M. Muncie[7,8,13,15], Valerie M. Weaver[4,7,8,9,10,11,12,13], Zev J. Gartner[6,14,16], and Jeffrey O. Bush[1,2,3,4]

EPH/EPHRIN signaling is essential to many aspects of tissue self-organization and morphogenesis, but little is known about how EPH/EPHRIN signaling regulates cell mechanics during these processes. Here, we use a series of approaches to examine how EPH/EPHRIN signaling drives cellular self-organization. Contact angle measurements reveal that EPH/EPHRIN signaling decreases the stability of heterotypic cell:cell contacts through increased cortical actomyosin contractility. We find that EPH/EPHRIN-driven cell segregation depends on actomyosin contractility but occurs independently of directed cell migration and without changes in cell adhesion. Atomic force microscopy and live cell imaging of myosin localization support that EPH/EPHRIN signaling results in increased cortical tension. Interestingly, actomyosin contractility also nonautonomously drives increased EPHB2:EPHB2 homotypic contacts. Finally, we demonstrate that changes in tissue organization are driven by minimization of heterotypic contacts through actomyosin contractility in cell aggregates and by mouse genetics experiments. These data elucidate the biomechanical mechanisms driving EPH/EPHRIN-based cell segregation wherein differences in interfacial tension, regulated by actomyosin contractility, govern cellular self-organization.

Introduction

Embryo morphogenesis requires the self-organization of cells into discrete regions, leading to the formation and maintenance of embryonic boundaries—interfaces that prevent cell intermixing to support patterning, maintain organization, and often, drive tissue separation (Fagotto, 2014). EPH/EPHRIN signaling plays a critical role in mediating tissue organization and is particularly important in establishing embryonic boundaries. The molecular mechanisms by which EPH/EPHRIN signaling directs tissue self-organization and boundary formation has been extensively studied in numerous systems. However, the biomechanical mechanisms underlying these processes remain unclear.

EPH receptors, and their signaling partners the membrane-bound EPHRINs, are expressed in most tissues of the vertebrate embryo and are often expressed in complementary domains. EPH/EPHRIN signaling mediates boundary formation by driving segregation between EPHRIN-expressing and EPH-expressing cells in many developmental contexts, including the germ layers during gastrulation, rhombomeres, somites, limb buds, cranial sutures, and intestinal crypts (Calzolari et al., 2014; Watanabe et al., 2009; Cooke et al., 2001; Batlle et al., 2002; Merrill et al., 2006; Rohani et al., 2011; Ting et al., 2009). At least one human congenital disease, craniofrontonasal syndrome, is caused by aberrant EPH/EPHRIN-based cell segregation (Kindberg and Bush, 2019; Twigg et al., 2004; O'Neill et al., 2016; Niethamer et al., 2020, 2017), and misregulation of EPHs and EPHRINs has been implicated in cancer metastasis (Pasquale, 2010; Batlle and Wilkinson, 2012; Porazinski et al., 2016). There are two subclasses of EPHRINs: A-type, which are membrane bound by a glycosylphosphatidylinositol anchor, and B-type, which are transmembrane and contains an intracellular cytoplasmic tail (Gale et al., 1996; Kullander and Klein, 2002).

[1]Program in Craniofacial Biology, University of California, San Francisco, San Francisco, CA; [2]Department of Cell and Tissue Biology, University of California, San Francisco, San Francisco, CA; [3]Institute for Human Genetics, University of California, San Francisco, San Francisco, CA; [4]Eli and Edythe Broad Center of Regeneration Medicine and Stem Cell Research, University of California, San Francisco, San Francisco, CA; [5]Biomedical Sciences Graduate Program, University of California, San Francisco, San Francisco, CA; [6]Department of Pharmaceutical Chemistry, University of California, San Francisco, San Francisco, CA; [7]Center for Bioengineering and Tissue Regeneration, University of California, San Francisco, San Francisco, CA; [8]Department of Surgery, University of California, San Francisco, San Francisco, CA; [9]Department of Bioengineering and Therapeutic Sciences, University of California, San Francisco, San Francisco, CA; [10]Department of Anatomy, University of California, San Francisco, San Francisco, CA; [11]Department of Radiation Oncology, University of California, San Francisco, San Francisco, CA; [12]UCSF Comprehensive Cancer Center, University of California, San Francisco, San Francisco, CA; [13]Helen Diller Family Cancer Research Center, University of California, San Francisco, San Francisco, CA; [14]Center for Cellular Construction, University of California, San Francisco, San Francisco, CA; [15]Graduate Program in Bioengineering, University of California, San Francisco, and University of California, Berkeley, San Francisco, CA; [16]Chan Zuckerberg Biohub, San Francisco, CA.

Correspondence to Jeffrey O. Bush: jeffrey.bush@ucsf.edu.

Because both EPH receptors and EPHRIN ligands are membrane bound, cell:cell contact is required for signaling, which can be transduced bidirectionally. "Forward" signaling occurs through activation of the EPH receptors, while "reverse" signaling is facilitated by adaptor proteins that bind to conserved phosphorylated tyrosines on the intracellular domain of B-type EPHRINs or to a C-terminal PDZ-binding domain. Forward signaling can occur through both kinase-dependent and kinase-independent mechanisms (Kullander and Klein, 2002; Niethamer and Bush, 2019).

Several hypotheses have been proposed for how EPH/EPHRIN signaling drives segregation and boundary formation between cell populations. Cell/cell repulsion, wherein cell:cell contact between EPH- and EPHRIN-expressing cells triggers migration of the EPH cell away from the repulsive EPHRIN source, is a long-standing hypothesis for EPH/EPHRIN-mediated cell segregation (Poliakov et al., 2008; Taylor et al., 2017; Mellitzer et al., 1999; Wu et al., 2019). This phenomenon is readily observed in culture at low cell density. Upon contact with an EPHRIN-expressing cell, the interface of the EPH-expressing cell mediating contact will collapse and retract away from the EPHRIN-expressing cell (Poliakov et al., 2008; O'Neill et al., 2016; Taylor et al., 2017; Astin et al., 2010). Cell segregation of fully intermixed cells by this mechanism would require repeated directional repulsion and migration of cells away from heterotypic contacts, resulting in an increased total migratory distance. However, we have observed that at high densities, segregation occurs without an increase in the migratory distance traveled, an observation inconsistent with this repulsive migration hypothesis (O'Neill et al., 2016).

Regulation of differential adhesion is a second hypothesis for how EPH/EPHRIN signaling drives cell segregation. According to the classical differential adhesion hypothesis, cells maximize their adhesive contacts to cluster hierarchically based on adhesive differences: The most adhesive cell population will cluster internally and be surrounded by less adhesive populations (Duguay et al., 2003; Steinberg and Takeichi, 1994; Steinberg, 1963; Foty and Steinberg, 2005). Differences in adhesive strength, also known as adhesion tension, between populations can be achieved through differing levels of cell adhesion molecule expression, termed differential adhesion, or through the type of cell adhesion molecule expressed, termed selective adhesion. There is evidence that EPH/EPHRIN signaling can modulate adhesion, including the ability of EPH activation to recruit ADAM10 metalloprotease, which cleaves E-cadherin, resulting in cadherin shedding and a decrease in cell:cell adhesion at the cell surface engaged in active EPH/EPHRIN signaling (Solanas et al., 2011).

Regulation of actomyosin contractility (e.g., differential cortical tension) also contributes to cell segregation (Harris, 1976) and provides a unifying explanation for these processes when combined with the notion of differential adhesion (Krieg et al., 2008; Maître et al., 2012; Cerchiari et al., 2015; Winklbauer, 2015). The resulting differential interfacial tension hypothesis states that forces arising from cell adhesion and cortex tension act in opposition to modulate the ability of cells to make stable contacts (Lecuit and Lenne, 2007; Brodland, 2002; Krieg et al., 2008). In recent years, it has come to be appreciated that the cell contact forces provided by cadherin-based adhesion tension are relatively small compared with those from cortical tension and that the role of cadherins in cell segregation is instead primarily to mechanically couple the contractile cell cortices to transduce actomyosin-generated forces (Maître et al., 2012; Maître and Heisenberg, 2013; Stirbat et al., 2013; Winklbauer, 2015; Lecuit and Yap, 2015). It should also be noted that cadherins and actomyosin contractility modulate each other biochemically to dynamically regulate adhesion tension and cortical contractility (Maître and Heisenberg, 2013; Lecuit and Yap, 2015; Slováková et al., 2020 *Preprint*). The balance of forces determines the mechanical potential of each interface; low-tension interfaces are favored over high-tension interfaces. According to the differential interfacial tension model, cell segregation minimizes the overall interfacial tension of the tissue. Thus, if a population of cells has a high interfacial tension at the cellular interface, it will be less able to form stable contacts with neighboring cells, resulting in the segregation of populations (Krieg et al., 2008; Brodland and Chen, 2000). However, the amount of contact at the cell:cell interface is also determined by the relative tension of the cortex away from the contact, known as the cell:medium cortical tension (Maître et al., 2012). Whereas in vitro cell/medium interactions involve all the cell–non-cell interactions (e.g., substrate and liquid medium), in vivo, cell:medium interactions are constituted by whatever surrounds the organizing cells (this can be ECM, fluid, yolk, or other cells; Cerchiari et al., 2015; Krieg et al., 2008; Maître et al., 2012). Further, cells dynamically regulate these forces through the action of signaling molecules acting at each interface. Currently, how upstream signaling pathways regulate cell:cell and cell:medium tension is largely unknown; specifically, how EPH/EPHRIN signaling regulates interfacial tension to achieve cell segregation is not clear.

While the role of EPH/EPHRIN signaling in differential interfacial mechanics is poorly understood, much is known about EPH/EPHRIN signaling as a regulator of actomyosin contractility. Actin accumulation and phosphorylated myosin light chain (MLC) are frequently observed at the interface between EPH/EPHRIN boundaries, including rhombomere boundaries, aberrant boundaries in the craniofacial mesenchyme, and in mesenchymal and epithelial cell culture (O'Neill et al., 2016; Calzolari et al., 2014; Cayuso et al., 2019; Rodríguez-Franco et al., 2017). Further, disruption of EPH/EPHRIN signaling leads to a loss of actin accumulation and phosphorylated MLC at these interfaces. However, how EPH/EPHRIN-driven actomyosin contractility contributes to initial segregation or to the maintenance of segregated cell populations is not known. Further, how EPH/EPHRIN signaling generally impacts the physical properties of cells to mediate cell segregation has not been examined.

Here, we ask how EPH/EPHRIN signaling regulates the biophysical properties of cells to modulate their ability to maintain stable cell:cell contacts during tissue organization. We use a HEK293 cell culture system in which EPHRIN-B1 and EPHB2 expression in two separate populations of cells drive robust segregation (Poliakov et al., 2008; O'Neill et al., 2016). We specifically examine how EPH/EPHRIN signaling impacts individual cell:cell contacts under conditions designed to minimize the role of cell migration. By examining isolated cell pairs,

performing live cell imaging of MLC localization, and using atomic force microscopy (AFM), we determine that EPH/EPHRIN signaling raises interfacial tension and decreases cell contact through increasing cortical actomyosin contractility. Surprisingly, we find that EPH/EPHRIN signaling also impacts homotypic cell contact through a cell:medium effect on cortical tension. Our findings support a view of segregation driven by minimization of overall interfacial tension both in vitro and in vivo.

Results

EPH/EPHRIN signaling increases heterotypic interfacial tension

To measure the effect of EPH/EPHRIN signaling on interfacial tension, we used a cell:cell contact angle assay to measure isolated cellular contacts between EPHRIN-B1– and EPHB2-expressing HEK293 cells in the absence of confounding effects of cell migration and cell-matrix adhesion (Cerchiari et al., 2015). We collected cell pairs in 20-µm by 40-µm agarose microwells made from polydimethylsiloxane (PDMS) stamps designed to allow two cells to adhere only to one another but not the substrate and measured the subsequent angle of cell contact (Θ) as an estimate of interfacial tension (Fig. 1 A; Cerchiari et al., 2015; Maître et al., 2012). We mixed HEK293 cells expressing EPHB2 and membrane-localized GFP (EPHB2-GFP) with cells expressing EPHRIN-B1 and LifeAct-mCherry (EPHRIN-B1-LifeAct-mCherry) and quantified interfacial tension at 4 h after mixing (Fig. S1 A). This time point was chosen based on a time course that showed stabilization of WT HEK293 cell contacts at 4 h after pairing in microwells. Our analysis revealed a significantly decreased contact angle between heterotypic EPHB2:EPHRIN-B1 cell pairs, while homotypic EPHRIN-B1:EPHRIN-B1 and EPHB2:EPHB2 cell pairs maintained close contact, indicating an increase in interfacial tension only at the heterotypic, EPHB2:EPHRIN-B1 interface (Fig. 1, B and C). When we live imaged cell pairs over 12 h, we observed that heterotypic EPHB2:EPHRIN-B1 cell pairs moved between extreme states of sparse and close contact throughout the time course (Fig. 1 D, Fig. S1 B, and Videos 1, 2, 3, and 4). However, considered across the entire population of cells measured, high heterotypic interfacial tension was consistent at any given time point, despite contacts being dynamic over time, indicating that heterotypic cell pairs favored sparse contact while homotypic pairs favored close contact (Fig. 1, C and D; and Fig. S1 C). This increased interfacial tension between heterotypic cell pairs was greatly diminished when signaling was blocked using exogenous unclustered EPHRIN-B1-Fc as a competitor of EPH/EPHRIN signaling (Fig. 1 C). Cell contact between WT and EPHB2-GFP cells was similar to that observed in WT:WT cell pairs, indicating that changes in interfacial tension for EPHRIN-B1:EPHB2 cell pairs were a consequence of activation of EPH/EPHRIN signaling in trans (Fig. S1 D). Together, these data indicate that in these cells, the balance of adhesion, cell:cell, and cell:medium tension favors extensive cell contact in the absence of EPH/EPHRIN signaling and that EPH/EPHRIN signaling drives increased cell:cell interfacial tension, preventing heterotypic cell pairs from maintaining close, stable, cell:cell contacts.

Hierarchy of segregation is consistent with high EPHB2:EPHRIN-B1 cellular interfacial tension

We next examined how EPH/EPHRIN-driven cell segregation occurs in 3D. Based on the premise that cells minimize high-energy contacts, hierarchy experiments in which two populations are mixed and the pattern of segregation is analyzed in 3D culture have been used to determine whether cell:cell contacts or cell:medium contact is relatively favorable (Krieg et al., 2008; Brodland and Chen, 2000). We performed 3D segregation experiments by mixing EPHB2-GFP-LifeAct-mCherry cells and EPHRIN-B1-LifeAct-mCherry cells into 180-µm circular agarose microwells. These cells robustly segregated, and rather than one cell type segregating to the center and being surrounded by the second cell type, as would be predicted by either differential adhesion or cell:medium tension that exceeds cell:cell tension, the two populations segregated completely and minimized contact with one another (Fig. 1 E). This is consistent with our cell contact angle measurements that show a high interfacial tension at the EPH/EPHRIN interface, and thus, this high-energy interaction at the EPH/EPHRIN cell:cell interface overcomes cellular cell:medium tension forces that would otherwise contribute to organizing the cells hierarchically.

Actomyosin contractility but not cadherin-mediated adhesion is critical to establish and maintain cellular self-organization

We previously demonstrated that EPH/EPHRIN-driven segregation can be disrupted, although not completely abolished, by inhibiting components of the actomyosin contractility pathway, such as rho-kinase (ROCK) or MLC kinase (MLCK; O'Neill et al., 2016). We further investigated how actomyosin contractility contributes to cell segregation by performing cell-mixing experiments in the presence of multiple actomyosin contractility pathway inhibitors and quantified cell sorting using nearest neighbor analysis, as previously described (Poliakov et al., 2008; O'Neill et al., 2016). Notably, when Y27632 (ROCK inhibitor) and ML7 (MLCK inhibitor) were added to the culture together, segregation was completely lost, with EPHB2-expressing and EPHRIN-B1–expressing cells remaining randomly intermixed (Fig. 2, A and B). This dual-inhibition condition did not affect the ability of the cells to migrate in culture because the total path length of these cells was not different from EPHRIN-B1:EPHB2 cells with DMSO (Fig. S2 A) and these cells were healthy because they were still able to segregate upon removal of inhibitors after 24 h (Fig. 2, A and D). As inhibition of actomyosin contractility could affect cell division, we asked whether inhibition of cell proliferation affected EPH/EPHRIN-driven cell segregation by mitomycin C treatment. Mitomycin C–treated cells still underwent robust segregation, indicating that proliferation does not play a critical role in EPH/EPHRIN-driven cell segregation (Fig. S2, C and D).

We next tested how classical cadherin-mediated adhesion might affect cell segregation. A recent study demonstrated that knockdown of N-cadherin does not abrogate cell segregation but leaves open possible compensation by other classical cadherins (Taylor et al., 2017). Classical cadherins depend on binding of extracellular calcium to rigidify the extracellular domains that enable binding of neighboring cadherins (Brasch et al., 2012).

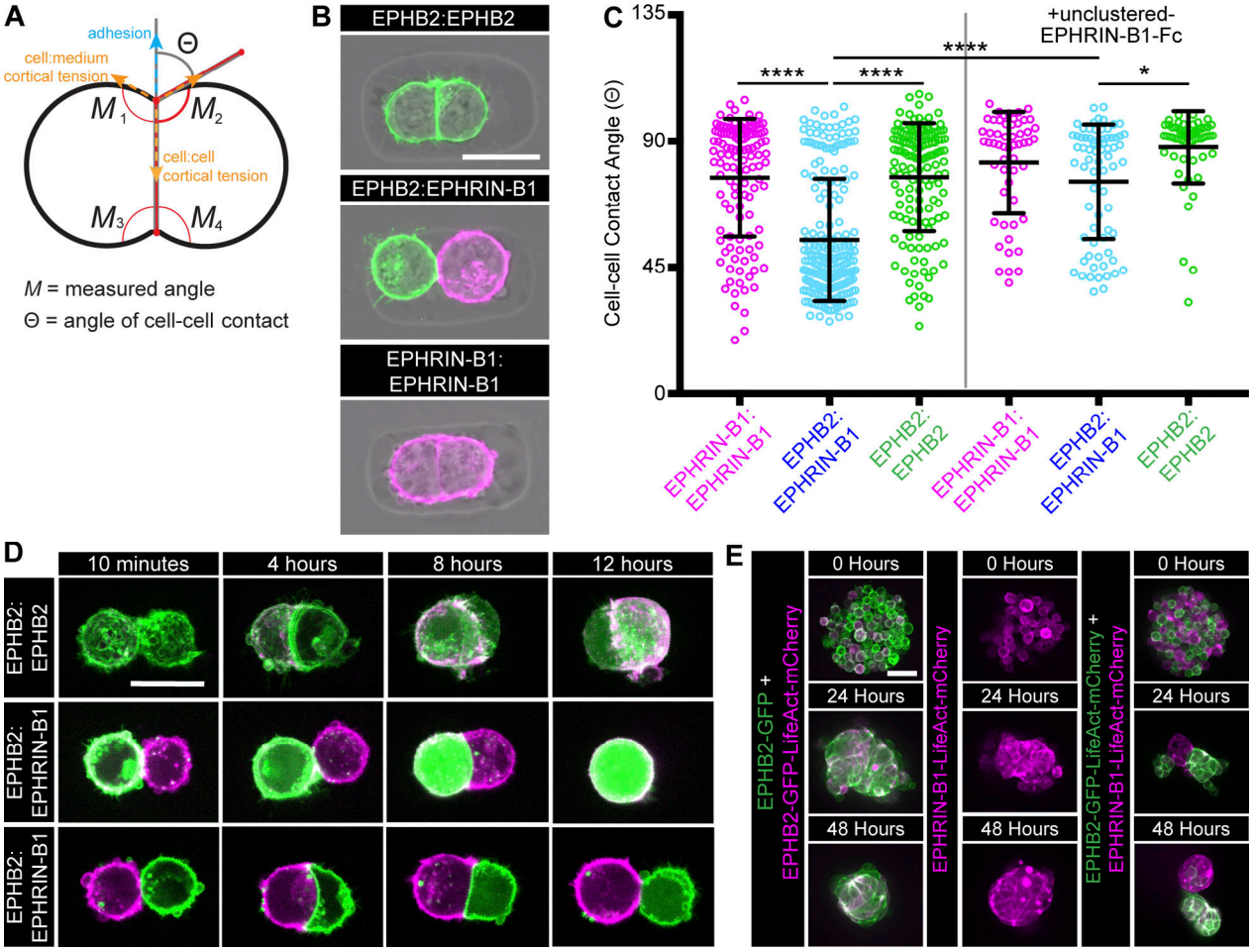

Figure 1. **EPH/EPHRIN signaling increases heterotypic interfacial tension. (A)** Schematic for cell:cell contact angle measurements. **(B)** Representative images of cell doublets in agarose microwells. EPHRIN-B1-mCherry (magenta) and EPHB2-GFP (green). Scale bars, 20 µm. **(C)** Quantification of cell:cell contact angles 4 h after plating. EPHB2:EPHRIN-B1 cell pairs show a decreased contact angle or increased interfacial tension. Upon the addition of unclustered-EPHRIN-B1-Fc, to block EPH/EPHRIN signaling, this relative increase in interfacial tension between heterotypic cell pairs is diminished. **(D)** Individual frames from live imaging experiments (Videos 1, 2, and 3) at 10 min, 4 h, 8 h, and 12 h of live imaging, showing that cell:cell contacts are dynamic over time. EPHRIN-B1-mCherry (magenta) and EPHB2-GFP-LifeAct-mCherry (green). Scale bars, 20 µm. **(E)** HEK293 3D cell aggregates in circular agarose microwells (180 µm). Scale bars, 50 µm. Error bars represent mean ± SD. *, P < 0.05; ****, P < 0.0001 (ANOVA followed by Dunnett's multiple comparison test).

We used cell culture medium without calcium (Ca^{2+}) to disrupt cadherin-based cell:cell adhesion, but we did not chelate intracellular calcium so as to minimize effects on intracellular Ca^{2+}-dependent functions (Bhagavathula et al., 2007; Yi et al., 2011). Indeed, in the cell:cell contact assay, this low-Ca^{2+} medium drastically reduced WT:WT cell:cell contacts (Fig. S2 B). Interestingly, we found that low-Ca^{2+} did not disrupt EPH/EPHRIN-driven cell sorting (Fig. 2, A and C), suggesting that sorting is independent of changes in cadherin-mediated adhesion.

In various contexts, actomyosin enrichment is observed at EPH/EPHRIN boundaries once segregation has occurred (Calzolari et al., 2014; Cooke et al., 2001; O'Neill et al., 2016; Taylor et al., 2017). To determine whether actomyosin contractility is required to maintain separate EPH-expressing and EPHRIN-expressing compartments, we applied actomyosin contractility inhibitors to cultures after segregation had already occurred. When Y27632 and ML7 were added together 24 h after mixing, significant remixing of EPHB2-expressing cells and EPHRIN-B1–expressing cells occurred by 48 h (Fig. 2, A and D). This result would not be expected if these inhibitors blocked actomyosin-dependent cell migration and demonstrates that actomyosin contractility is critical for maintaining EPH/EPHRIN boundaries by minimizing EPH/EPHRIN cell intermixing. These data demonstrate that actomyosin contractility is not only critical for driving increased interfacial tension at the heterotypic cell:cell interface but also necessary for establishing and maintaining cellular organization without impacting cell migration in this system, while regulation of cadherin-mediated adhesion is not essential for this process.

EPH/EPHRIN signaling increases cortical tension and requires actomyosin contractility to increase interfacial tension

To determine whether increased cell:cell interfacial tension between heterotypic cell pairs is attributed to actomyosin contractility, we performed cell:cell contact angle assays in the presence of well-characterized inhibitors of the actomyosin

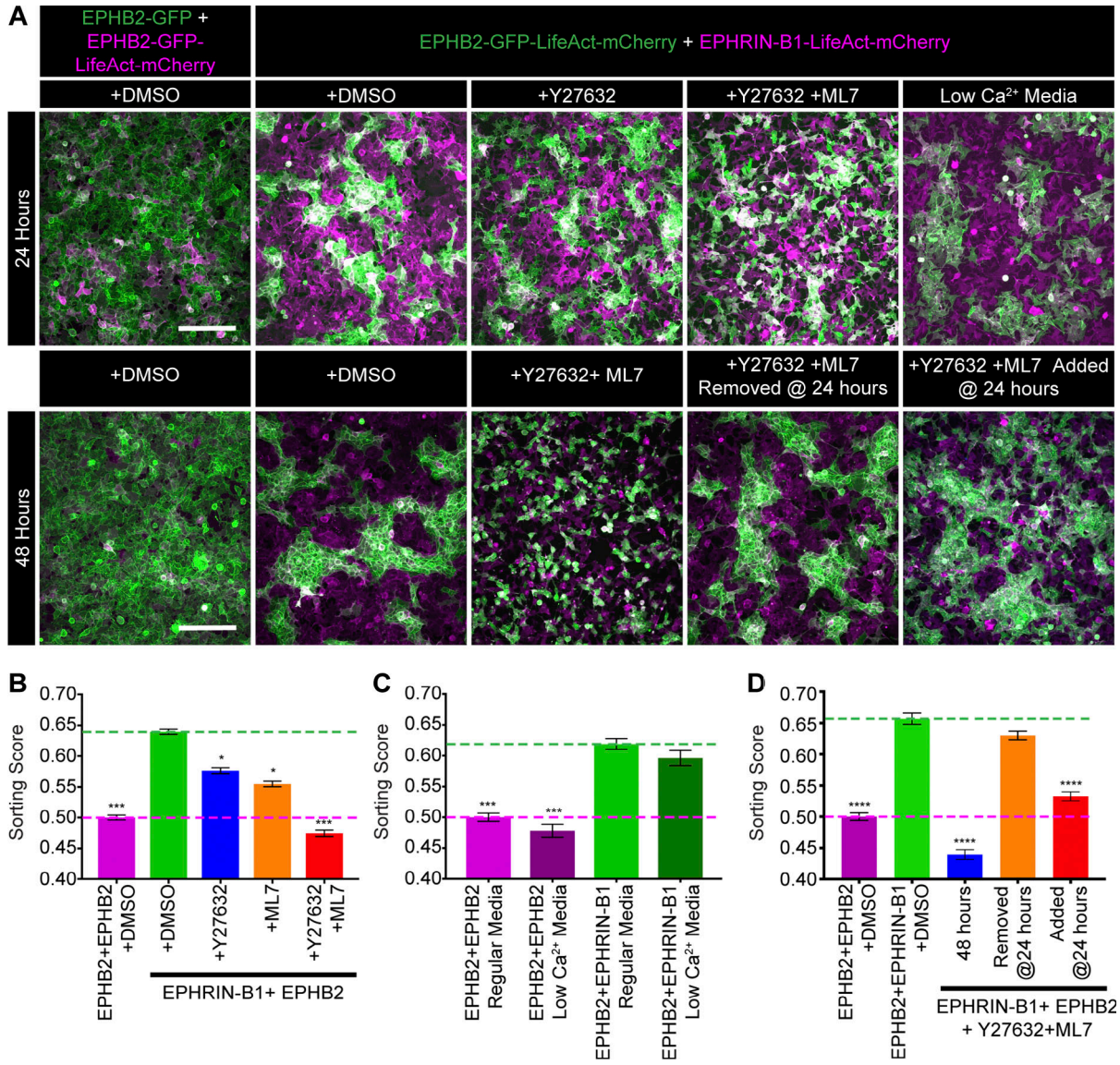

Figure 2. **Cell segregation is abolished by dual inhibition of ROCK and MLCK. (A)** Cell segregation in mixed populations of HEK293 cells. In the far-left panels EPHB2-GFP (green) cells were mixed with EPHB2-GFP-LifeAct-mCherry (magenta) cells. In the rest of the panels, EPHB2-GFP-LifeAct-mCherry (green) cells were mixed with EPHRIN-B1-mCherry (magenta) cells and treated with vehicle (DMSO) or inhibitors or cultured in low-Ca^{2+} media to determine effect on cell segregation. For images at 48 h, some inhibitors were added or removed at 24 h. Scale bars, 200 µm. **(B)** Quantification of cell segregation for several of the conditions illustrated in (A). Dual inhibition of ROCK and MLCK abolished cell segregation. **(C)** Quantification of cell segregation in the absence of calcium. Cell segregation was undisrupted by the lack of calcium in the media. **(D)** Quantification of cell segregation upon the addition or removal of inhibitors. Cell segregation is still able to occur upon removal of ROCK and MLCK inhibitors after 24 h, and addition of these inhibitors to media at 24 h after sorting disrupts cell segregation. Cell segregation was quantified using the nearest neighbor method. Column heights represent means of the technical replicates, and error bars represent SEM. Results are representative of three experiments. *, $P < 0.05$; ***, $P < 0.001$; ****, $P < 0.0001$ versus (B) EPHB2 + EPHRIN-B1 + DMSO condition, (C) EPHB2 + EPHRIN-B1 regular media condition, and (D) EPHB2 + EPHRIN-B1 + DMSO condition at 48 h (ANOVA followed by Dunnett's multiple comparison test).

contractility pathway. Blebbistatin, an inhibitor of myosin II ATPase activity, significantly diminished heterotypic interfacial tension (Fig. 3, A and B), with increased contact between EPHB2: EPHRIN-B1 cell pairs, more similar to what we observed in homotypic cell pairs or when EPH/EPHRIN signaling was blocked. We confirmed this relaxation of interfacial tension using other inhibitors of actomyosin contractility pathways, including dual inhibition by Y27632 and ML7 (Fig. 3, A and B). These data show that actomyosin contractility is required for EPH/EPHRIN heterotypic interfacial tension and modulates the ability of these cells to generate stable contacts.

Modulating the balance between contractility and adhesion would be expected to change cell contact regardless of whether EPH/EPHRIN signaling acts directly to impact adhesion or cortical actomyosin contractility (Maître et al., 2012; Lecuit and Lenne, 2007). To determine whether EPH/EPHRIN signaling changes cortical contractility, we performed AFM to measure the mechanical stiffness of EPHB2- or EPHRIN-B1–expressing

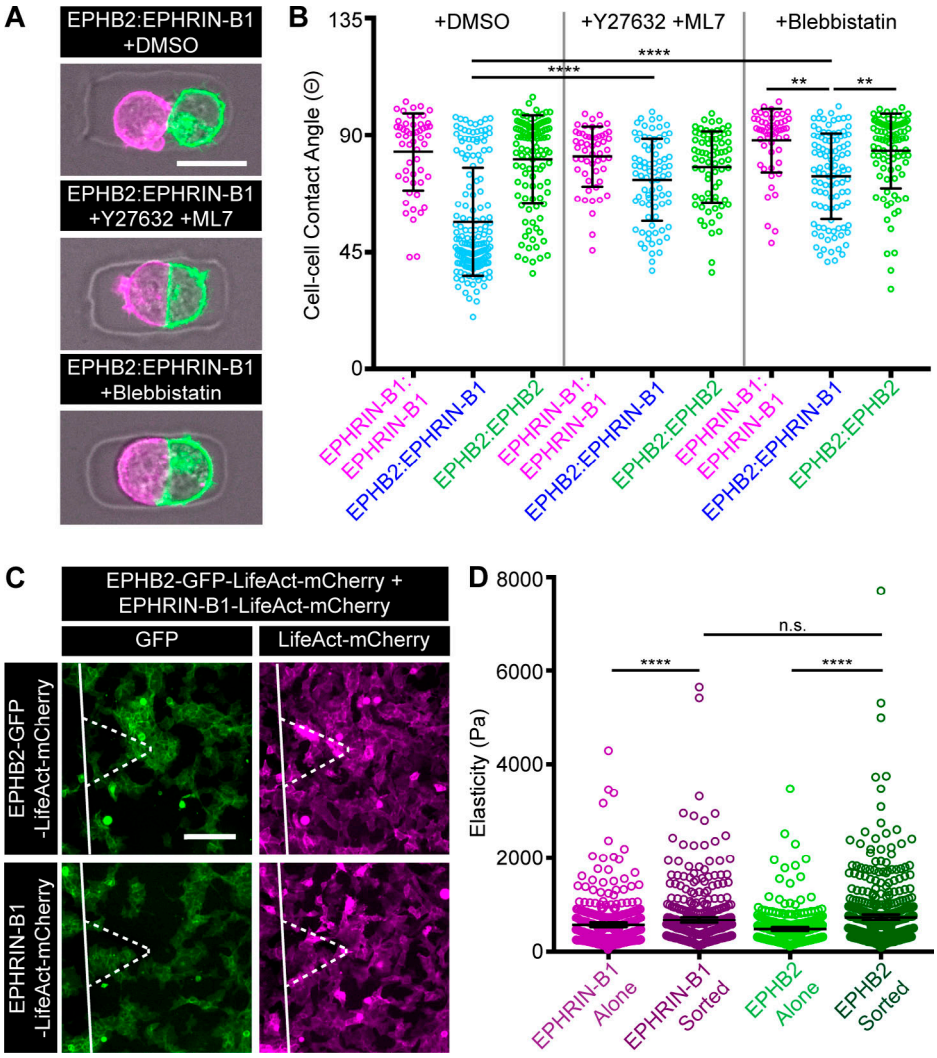

Figure 3. **Actomyosin contractility drives increased cellular interfacial tension. (A)** Representative images of cell doublets in agarose microwells. EPHRIN-B1-mCherry (magenta) and EPHB2-GFP (green) treated with vehicle (DMSO) or inhibitors. Scale bar, 20 µm. **(B)** Quantification of cell:cell contact angles 4 h after plating. In HEK293 media with DMSO, EPHB2:EPHRIN-B1 cell pairs show a decreased contact angle compared with EPHRIN-B1:EPHRIN-B1 homotypic cell pairs or EPHB2:EPHB2 homotypic cell pairs. Upon the addition of Y27632 and ML7 or the addition of blebbistatin, EPHB2:EPHRIN-B1 cell pairs no longer show diminished contact compared with EPHB2:EPHRIN-B1 cell pairs in media with DMSO control. Error bars represent mean ± SD. **, $P < 0.01$; ****, $P < 0.0001$ (ANOVA followed by Dunnett's multiple comparison test). **(C)** Representative images of EPHRIN-B1-mCherry (magenta) cells and EPHB2-GFP (green) cells mixed and segregated after 24 h, when AFM was performed. White outline represents location of AFM machinery in each image. Scale bar, 200 µm. **(D)** Quantification of cellular elasticity (Pa) determined by AFM either when EPHRIN-B1 or EPHB2 cells were cultured alone or when these cells were mixed and allowed to segregate. Both cell types in sorted conditions show increased stiffness compared with when cultured alone. Error bars represent mean with 95% CI. ****, $P < 0.0001$ (ANOVA followed by Dunnett's multiple comparison test).

cells when cultured alone or when mixed and undergoing cell segregation for 24 h (Fig. 3 C). In mixed cultures, we probed regions of EPHB2-GFP or EPHRIN-B1-LifeAct-mCherry and compared these with control cultures grown alone. Notably, we found an increase in stiffness of both EPHB2 cells and EPHRIN-B1 cells when undergoing cell segregation in mixed cultures compared with either population alone, suggesting that EPH/EPHRIN signaling increases actomyosin cortical tension during cell segregation (Fig. 3 D). We observed an increase in stiffness at 4 h following mixing of EPHB2 and EPHRIN-B1 cells, and before any sorting was visible, indicating that this increased cortical actomyosin contractility was a consequence of EPH/EPHRIN signaling rather than a consequence of cell segregation (Fig. S3, A and B). As expected, inhibition of actomyosin contractility with Y27632 and ML7 resulted in a significant decrease in cellular stiffness across EPHB2- and EPHRIN-B1–expressing cells compared with sorted controls (Fig. S3 C). Taken together, these results indicate that increased cortical contractility at heterotypic cell:cell interfaces disrupts the ability of EPH-expressing and EPHRIN-expressing cells to maintain stable contacts, thereby dictating cellular organization during segregation based on minimization of heterotypic contacts.

Myosin localizes at heterotypic contacts

Contractile forces generated by the actomyosin cytoskeleton are driven by the activity of myosin on actin filaments. To determine

whether actomyosin contractility is increased at heterotypic interfaces, we visualized the localization of myosin light chain at heterotypic and homotypic contacts in HEK293 cell lines expressing EPHB2 and EPHRIN-B1 as well as an MLC-cherry fusion protein (EPHB2-GFP-MLC-cherry and EPHRIN-B1-MLC-cherry; Videos 5, 6, 7, 8, 9, 10, 11, and 12). Upon contact with an EPHRIN-B1–expressing cells, EPHB2 cells show an increase in MLC at the EPH:EPHRIN contact interface (Fig. 4, C and E; Fig. S4 C; and Videos 7 and 11). This localized MLC is not observed in homotypic contacts or at heterotypic contacts in the presence of unclustered EPHRIN-B1-Fc (Fig. 4, A–E; Fig. S4, A–D; and Videos 5, 6, 8, 9, 10, and 12). These results indicate that EPH/EPHRIN signaling gives rise to localized increased myosin, further demonstrating that high heterotypic interfacial tension is driven by actomyosin contractility.

EPHB2 cells increase homotypic contacts by a cadherin-independent mechanism

It has been reported that EPHB2 cell groups condense during EPH/EPHRIN-driven cell segregation (Taylor et al., 2017). We interrogated whether EPH-EPHRIN signaling might also impact homotypic cell:cell contacts. We found that EPHB2 cells show an increased density after undergoing segregation compared with EPHRIN-B1– or EPHB2-expressing cells cultured alone, similar to the previous report (Taylor et al., 2017). Interestingly, the increase in EPHB2 cell density persisted in low-Ca^{2+} media conditions (Fig. 5, A and B; and Fig. S5 A and B), indicating that this condensation is independent of cadherin-based cell adhesion.

On the basis of this finding, we further investigated this adhesion-independent homotypic cell density effect by performing the cell:cell contact angle assay in the absence of calcium. As expected, in the absence of calcium-dependent adhesion, EPHRIN-B1 homotypic contacts decreased dramatically, indicating that cadherin-based adhesion likely drives homotypic contact between EPHRIN-B1–expressing cells (Fig. 5, C and D). Also unsurprisingly, heterotypic EPHRIN-B1:EPHB2 cell pairs retained limited contact in the absence of calcium, with additional loss of the high-contact subpopulation, suggesting a loss of dynamic oscillation between high- and low-contact states (Fig. 5, C and D). However, EPHB2 homotypic pairs retained close contact, even in the absence of calcium-dependent adhesion (Fig. 5, C and D). Given our findings indicating that calcium-mediated adhesion does not play an important role in cellular self-organization and that EPHB2 cells increase their homotypic affinity independent of calcium-dependent adhesion, we examined whether EPH/EPHRIN signaling had nonautonomous effects on cellular organization. Whereas EPHB2-expressing cells readily mix with WT HEK293 cells labeled only with LifeAct-BFP (WT-LifeAct-BFP; Fig. S5 C), mixing EPHB2 cells with both WT-LifeAct-BFP and EPHRIN-B1–expressing cells resulted in nearly complete exclusion of WT-LifeAct-BFP cells from EPHB2 cell clusters; WT-LifeAct-BFP instead intermixed with EPHRIN-B1 cells (Fig. S5 C). These data indicate that upon receiving stimuli from EPHRIN-B1–expressing cells, EPHB2 cells preferentially organize homotypically and prevent the invasion of signaling inert HEK293 cells.

The configuration of a cell:cell contact not only is due to the cell:cell interfacial tension but also is an outcome of the relative forces acting at the cell:cell interface and cell:medium interface (Maître et al., 2012; Brodland and Chen, 2000). Whereas high actomyosin contractility at the cell:cell interface limits stable contacts, high cell:medium interfacial tension driven by actomyosin contractility is minimized by driving increased cell:cell contact. To determine whether high cell:medium tension was driving increased EPHB2 homotypic cell contact, we measured the cell:cell contact angle in the absence of calcium and in the presence of blebbistatin to decrease cortical actomyosin contractility at both the cell:cell and the cell:medium interface (Fig. 5, C and D). We found that blocking actomyosin contractility in the absence of calcium-dependent adhesion decreased contact between EPHB2 homotypic cell pairs, suggesting that EPHB2-expressing cells have a high cell:medium interfacial tension driven by cortical actomyosin contractility away from the cell:cell interface (Fig. 5, C and D). Taken together, these data suggest that the EPH/EPHRIN-mediated cellular organization, with robust segregation between EPHB2- and EPHRIN-B1–expressing cells and increased density of EPHB2 cells, is a result of both increased heterotypic cell:cell interfacial tension and EPHB2 homotypic affinity driven by high cell:medium tension.

Actomyosin contractility is important for cell segregation in vivo

To determine whether increased actomyosin contractility at heterotypic cell interfaces drives cell segregation in vivo, we used a genetic mouse model that is mosaic for EPHRIN-B1. Mosaicism for mutations in X-linked EPHRIN-B1, arising from random X-inactivation around embryonic day 5.5 in heterozygous females, results in cell segregation between EPHRIN-B1–expressing and –nonexpressing cells in mice (Compagni et al., 2003; O'Neill et al., 2016; Niethamer et al., 2020; Bush and Soriano, 2010). To disrupt actomyosin contractility, we used mice carrying floxed alleles of nonmuscle myosin IIA (NMIIA) and NMIIB and a *Shox2*^{IresCre} allele to drive recombination and robust cell segregation in the anterior palate. We also included in these experiments an X-linked GFP transgene as an independent marker of the extent of cell segregation (Hadjantonakis et al., 1998). We observed robust cell segregation in the anterior palate of *Efnb1*$^{loxXGFP/+}$;*Shox2*$^{IresCre/+}$ embryos (Fig. 6 A), whereas *Efnb1*$^{loxXGFP/+}$;*NMIIA*$^{lox/lox}$;*NMIIB*$^{lox/lox}$;*Shox2*$^{IresCre/+}$ embryos exhibited disruption of cell segregation with smaller patches and more single, unsorted XGFP^{+} cells appearing throughout the palate (Fig. 6 A). We quantified the extent of cell segregation by counting the number of cells per XGFP^{+} patch and measuring the patch area, which revealed a significant decrease in XGFP^{+} patch size compared with *Efnb1*$^{loxXGFP/+}$;*Shox2*$^{IresCre/+}$ embryos (Fig. 6, B and C). These data demonstrate the importance of actomyosin contractility in driving cell segregation in vivo.

Cell segregation by EPH/EPHRIN signaling affects tissue morphology

Boundaries between EPH- and EPHRIN-expressing populations are critical for tissue separation and morphogenesis in numerous contexts, including germ layer separation, somites, and rhombomeres (Calzolari et al., 2014; Watanabe et al., 2009;

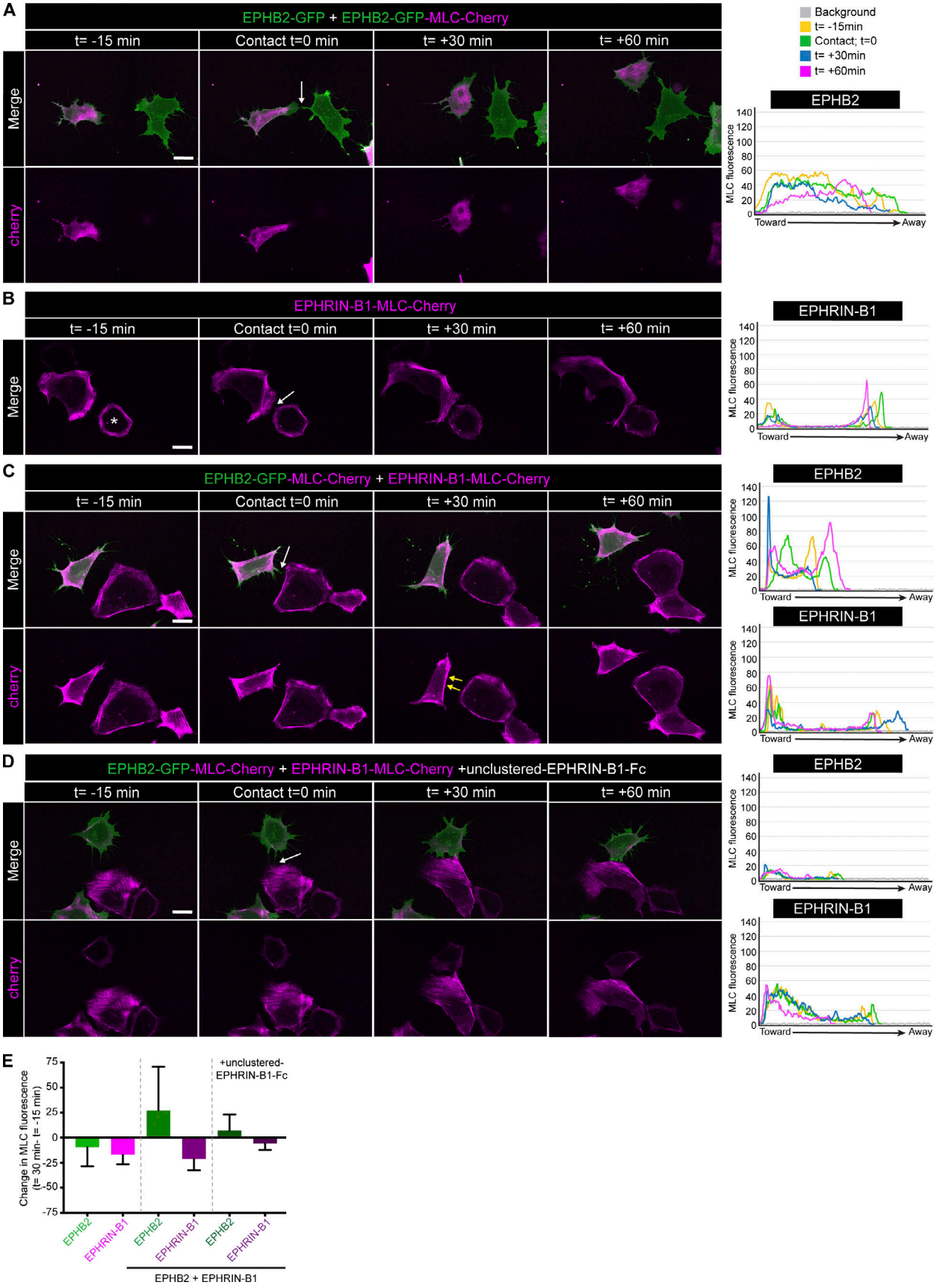

Figure 4. **MLC localization increases at heterotypic contacts. (A)** Example images from live imaging experiments (Video 5) of EPHB2 homotypic conditions at low density. EPHB2-GFP (green) cells were mixed with EPHB2-GFP-MLC-Cherry (magenta). Line scan analysis of cell pair at various time points shows no

change in MLC localization upon contact. **(B)** Example images from live imaging experiments (Video 6) of EPHRIN-B1 homotypic conditions at low density. EPHRIN-B1-MLC-Cherry (magenta). The asterisk indicates the analyzed cell. Line scan analysis of the cell pair at various time points shows no change in MLC localization upon contact. **(C)** Example images from live imaging experiments (Video 7) of heterotypic conditions at low density. EPHB2-GFP-MLC-Cherry (green) cells were mixed with EPHRIN-B1-MLC-Cherry (magenta) cells. Yellow arrows at t = 30 min indicate localized increase in MLC. Line scan analysis of the cell pair at various time points shows that MLC localized to cell contact in EPHB2 cells upon contact. **(D)** Example images from live imaging experiments (Video 8) of heterotypic, with unclustered-EPHRIN-B1-Fc, conditions at low density. EPHB2-GFP-MLC-Cherry (green) cells were mixed with EPHRIN-B1-MLC-Cherry (magenta) cells; unclustered-EPHRIN-B1-Fc was added to prevent signaling. Line scan analysis of the cell pair at various time points shows no change in MLC localization upon contact. **(E)** Quantification of the change in MLC fluorescence from before contact (t = −15 min) to after contact (t = 30 min). EPHB2 cells show an increase in MLC localization at heterotypic interface upon contact with EPHRIN-B1–expressing cell. This effect is blocked by the addition of unclustered-EPHRIN-B1-Fc. Column heights represent mean, and error bars represent SD. White arrow at t = 0 min indicates point of contact. Toward indicates toward contact, while away indicates away from contact. Scale bars, 20 µm.

Cooke et al., 2001; Rohani et al., 2011). To determine in a simple system how the properties of heterotypic and homotypic contact strength that we have uncovered here influence larger-scale organization and tissue shape, we performed cell segregation assays in 3D hanging drop culture. In control aggregates, where EPHB2-GFP cells were mixed with EPHB2-GFP-LifeAct-mCherry cells, cells intermixed, and the overall morphology appeared spherical and smooth. However, when EPHB2-GFP-LifeAct-mCherry cells were mixed with EPHRIN-B1-LifeAct-mCherry cells, cells segregated, and the morphology of the aggregates was highly irregular and tortuous (Fig. 7 A). Because it was difficult to determine how the tortuous morphology correlated with boundary formation in these large aggregates, we also generated smaller aggregates by isolating small groups of cells 24 h after cell mixing and culturing these aggregates in isolation for an additional 24–48 h (Fig. S6 A). Consistent with our earlier cell sorting assays in circular microwells (Fig. 1 E), we observed that the EPHB2 and EPHRIN-B1 cell populations minimize their

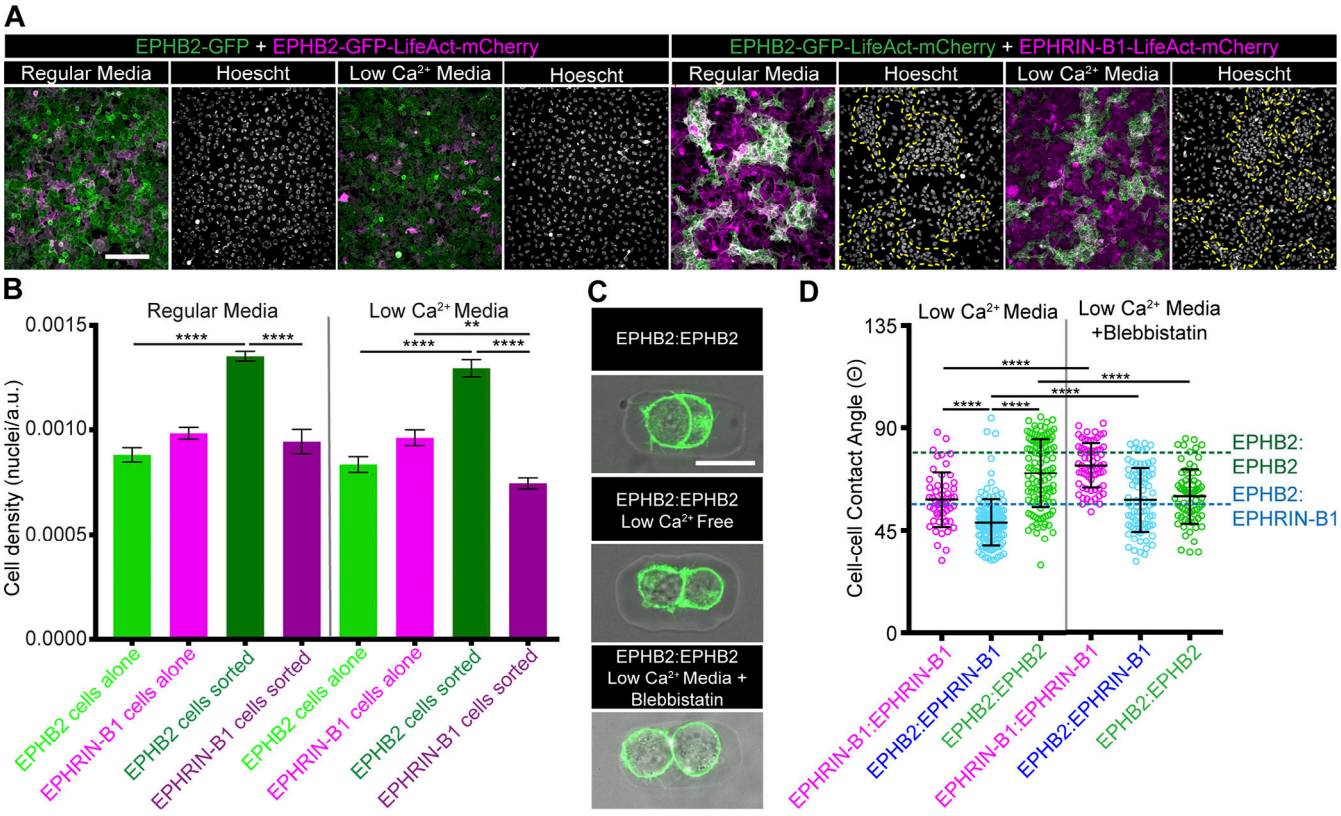

Figure 5. **EPHB2 cells increase homotypic contacts due to high cell:medium cortical tension. (A)** Cell segregation in mixed populations of HEK293 cells. In the left panels, EPHB2-GFP (green) cells were mixed EPHB2-GFP-LifeAct-mCherry (magenta) cells in either regular or low-Ca^{2+} media. In the right panels, EPHB2-GFP-LifeAct-mCherry (green) cells were mixed with EPHRIN-B1-LifeAct-mCherry (magenta) cells in regular HEK293 or low-Ca^{2+} media. Hoescht images shown to visualize nuclei. Yellow dashed lines outline EPHB2 cell patches. Scale bar, 200 µm. **(B)** Quantification of nuclear density for the conditions illustrated in (A). In both regular and low-Ca^{2+} media, EPHB2 cells have a significantly increased density. Column heights represent means of the technical replicates, and error bars represent SEM. **, P < 0.01; ****, P < 0.0001. **(C)** Representative images of cell doublets in agarose microwells. EPHB2-GFP (green). Scale bar, 20 µm. **(D)** Quantification of cell:cell contact angles in the absence of calcium. Cell:cell contacts diminish in the absence of calcium; however, EPHB2:EPHB2 homotypic contacts are somewhat retained. In low-Ca^{2+} media with the addition of blebbistatin, EPHB2:EPHB2 contacts are diminished. Dashed lines indicate average cell:cell contact angles in regular media conditions. Error bars represent mean ± SD. ****, P < 0.0001.

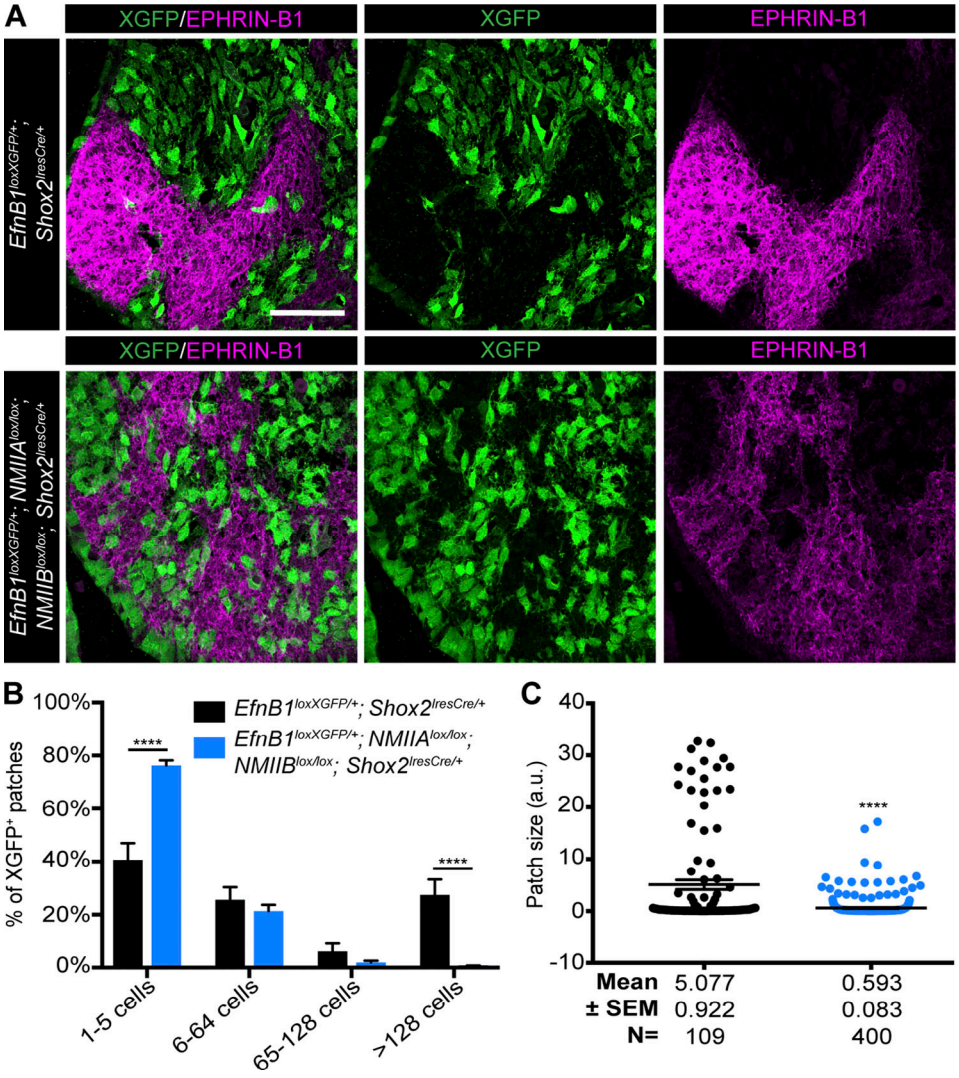

Figure 6. **Cell segregation in vivo is disrupted by lack of actomyosin contractility. (A)** Immunostaining of embryonic day 13.5 coronal sections for EPHRIN-B1 (magenta) and GFP (green) shows segregation in *EfnB1*$^{loxXGFP/+}$;*Shox2*$^{IresCre/+}$ embryos and diminished segregation when actomyosin contractility is disrupted in *EfnB1*$^{loxXGFP/+}$;*Shox2*$^{IresCre/+}$;*NMIIA*$^{lox/lox}$;*NMIIB*$^{lox/lox}$ embryos. Scale bar, 50 µm. **(B)** Distribution of the percentage of XGFP^{+} patches of various sizes. Column height represents means of the distributions across all sections measured for a given genotype; error bars represent SEM. **(C)** Patch sizes represented as scatterplots. Horizontal bars represent means, and error bars represent SEM. ****, P < 0.0001.

contact with one another, minimizing high-tension interactions and altering aggregate morphology at the point of heterotypic contact (Fig. 7 B). To determine whether these changes in morphology were also driven by actomyosin contractility, we added Y27632 and ML7 to this hanging drop assay. When these inhibitors were added to the culture medium at 24 h, a time point at which segregation had occurred, the morphology of the aggregate changed dramatically. The aggregates appeared much more spherical, and contact was no longer minimized at EPH/EPHRIN interfaces (Fig. 7 B). This was also true when inhibitors were added to large tortuous aggregates at 72 h and cultured for an additional 48 h (Fig. S6 B). These data show that actomyosin contractility driven by heterotypic EPH/EPHRIN cell contact not only governs cellular organization but also likely underlies the subsequent tissue separation shape changes that are often observed at EPH/EPHRIN boundaries in vivo.

Discussion

While long known to regulate cells' ability to intermix and self-organize, we now discover how EPH/EPHRIN signaling regulates cell contacts to drive cellular self-organization and boundary formation. The differential interfacial tension hypothesis predicts that cells minimize contacts with high mechanical potential (Brodland and Chen, 2000). These high-tension interfaces can occur between a cell and the medium, the matrix, or another cell population. The outcome of self-organization is therefore driven by the minimization of overall tension by increasing the relative surface area of low-tension interfaces at the expense of high-tension interfaces (Maître et al., 2012). Overall interfacial tension is dictated by a combination of adhesion and cortical tension, wherein the balance between cell:cell and cell:medium tensions modulate cell contact (Winklbauer, 2015). When tension is highest between heterotypic

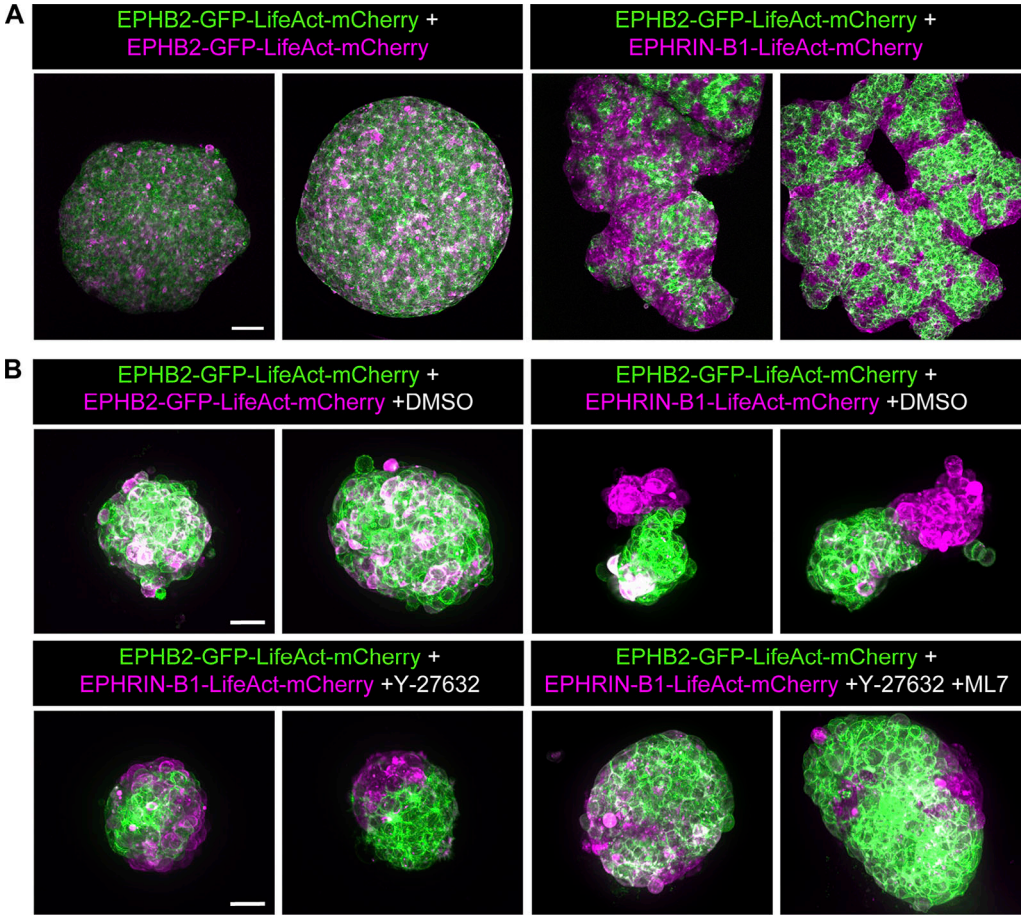

Figure 7. **EPH/EPHRIN signaling affects tissue morphology. (A)** In the left panels, representative images show that EPHB2-GFP (green) cells mixed with EPHB2-GFP-LifeAct-mCherry (magenta) cells in hanging drop cultures for 72 h form circular aggregates. In the right panels, EPHB2-GFP-LifeAct-mCherry (green) cells mixed with EPHRIN-B1-LifeAct-mCherry (magenta) cells in hanging drop cultures for 72 h segregate and form highly tortuous aggregates. Scale bar, 100 µm. **(B)** HEK293 cell–isolated aggregates formed in hanging drop cultures 72 h after mixing. Morphology changes observed in segregated aggregates are disrupted by inhibition of ROCK and MLCK with Y27632 and ML7. Scale bars, 50 µm.

cell types, cells minimize cell:cell contacts. Indeed, our data show that EPH/EPHRIN signaling results in increased relative cell:cell interfacial tension by modulating actomyosin contractility and cortical tension at heterotypic contacts, which results in cell segregation and boundary formation (Fig. 8, A and B). Consistent with this mechanism, cell segregation is abolished in vitro and highly disrupted in vivo when actomyosin contractility is disrupted and both EPHB2 and EPHRIN-B1 cells increase their stiffness when undergoing segregation.

If tension is highest at the cell:medium interface, cells minimize contact with the medium in favor of cell:cell interactions. Differential cell:medium cortical tension has been shown to drive cell segregation in zebrafish germ layer separation and mammary epithelium organization (Cerchiari et al., 2015; Krieg et al., 2008; Maître et al., 2012). In these systems, cells with the highest cell:medium interfacial tension aggregated at the center, thereby minimizing unfavorable, high interfacial tension interactions with the surrounding medium (Cerchiari et al., 2015; Krieg et al., 2008). The relative influence of cell:cell and cell:medium tension is reflected by 3D segregation hierarchy experiments where we observe that the two populations minimize their contact with one another rather than one population being enveloped by the other. However, whereas heterotypic EPH/EPHRIN interactions are the least energetically favorable interaction and dominate cellular organization, a secondary effect of cell:medium tension also contributes to self-organization by increasing contact between EPH-expressing cells (Fig. 8, A and B). In our experiments, the absence of cadherin-based adhesion revealed that EPHB2 homotypic cell contact is driven by cell:medium tension generated by actomyosin contractility rather than cell:cell adhesion tension. This discovery is somewhat surprising, as cadherins are thought to be required to mechanically couple the cortices of cells to enable cortical tension to regulate cell contact (Maître et al., 2012). The ability of EPHB2 homotypic signaling to expand cell contacts in low-Ca^{2+} conditions may therefore reflect that cadherin function is incompletely abrogated in our experiments, although we do not think this is the case because EPHRIN-B1:EPHRIN-B1 homotypic contacts and WT:WT homotypic contacts are dramatically reduced. Alternatively, our results may suggest the existence of a cadherin-independent adhesion mechanism for coupling cell cortices or more passive spreading of cells on one another, as

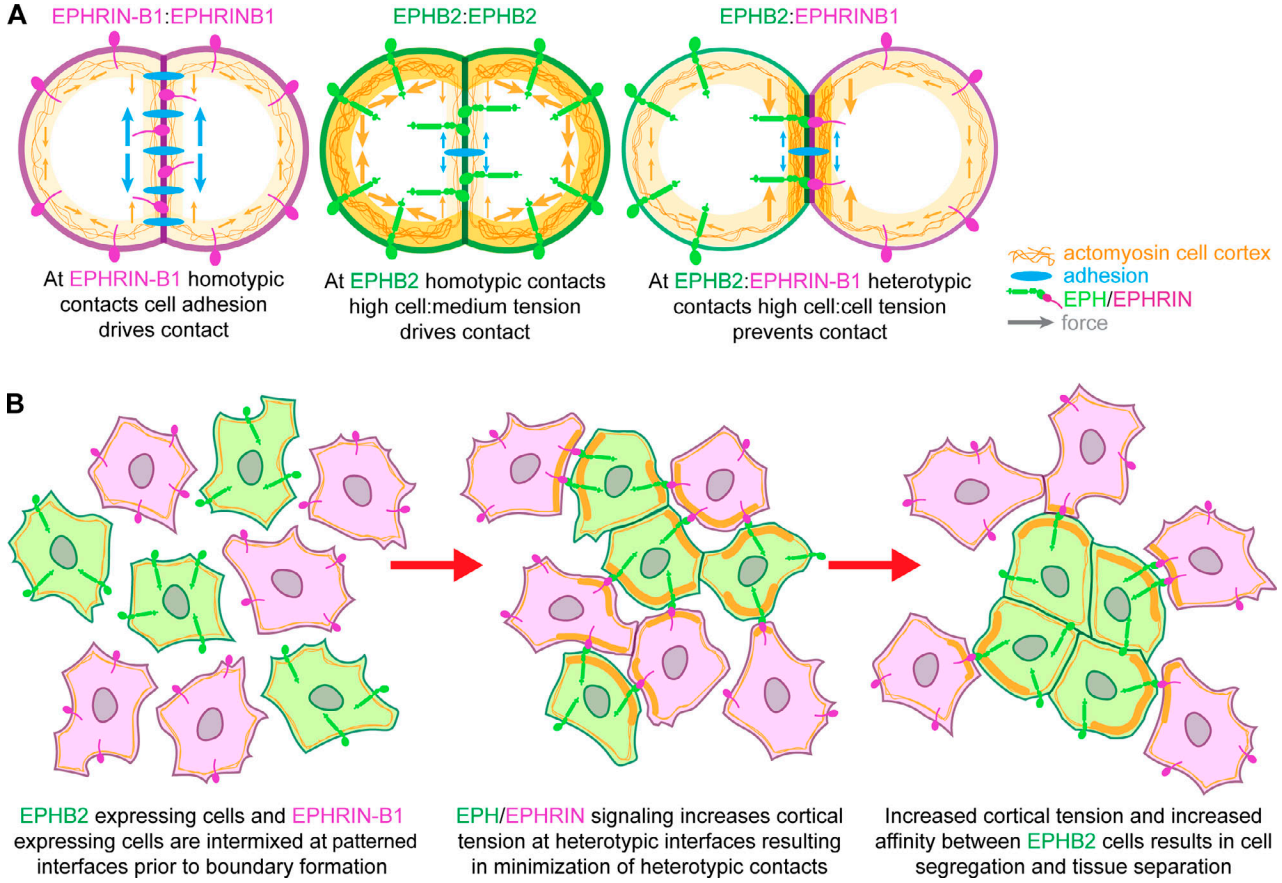

Figure 8. **EPH/EPHRIN signaling modulates both cell:cell and cell:medium tension, driven by actomyosin contractility to drive cellular organization.** **(A)** Schematic of cell:cell contacts and the forces that modulate these contacts. EPHB2:EPHB2 homotypic contact is driven by increased cell:medium tension, while EPHRIN-B1:EPHRIN-B1 homotypic contact is driven by cell adhesion. EPHB2:EPHRIN-B1 heterotypic cell pairs show high cell:cell interfacial tension due to increased actomyosin contractility at the cell:cell interface. **(B)** High cell:cell interfacial tension between EPHB2- and EPHRIN-B1–expressing cells results in a minimization of contact between these cell populations. Together with increased EPHB2 homotypic affinity, this increased cortical tension, preventing the formation of stable heterotypic contacts, drives cell segregation.

was previously demonstrated upon disruption of adherence junctions through removal of α-catenin (Stirbat et al., 2013).

High cell:cell interfacial tension has also been suggested to drive segregation in *Xenopus* at the mesoderm–endoderm boundary, although this effect was proposed to be independent of cortical tension (Canty et al., 2017). Our data support a model in which actomyosin contractility at the EPH/EPHRIN cell:cell interface prevents heterotypic cell pairs from maintaining stable contacts and thus segregating from one another, while homotypic contacts driven by cell:medium interfacial tension help to reinforce this interaction (Fig. 8, A and B). The pathways employed downstream of EPH/EPHRIN signaling to differentially regulate tension at the cell:cell and cell:medium interfaces will be an exciting future research question.

Because of the well-established role of EPH/EPHRIN signaling in mediating axon guidance via growth cone collapse, cellular guidance by repulsive migration has been a long-standing hypothesis for how EPH/EPHRIN signaling drives cell segregation and boundary formation. Indeed, EPH/EPHRIN-mediated repulsive migration has been observed in pairs of individual cells (Poliakov et al., 2008; Astin et al., 2010; O'Neill et al., 2016). Further, computer simulations of cell segregation using experimentally measured parameters of contact duration, frequency of cellular collapse, and migration away do show robust cell segregation, while in these same simulations, solely decreasing contact frequency between heterotypic cell pairs only drives mild cell segregation (Taylor et al., 2017). However, several observations do not support cell migration as a driver of cell segregation in our system. First, we previously showed that during cell segregation, EPHB2 cells decrease their total migratory distance rather than travel a greater distance as would be predicted by repetitive repulsive migration (O'Neill et al., 2016). Second, we do not see changes in migratory behaviors of cells when blocking actomyosin contractility and thus preventing segregation. Further, upon inhibition of actomyosin contractility after segregation has occurred, cells remix, indicating that inhibition of actomyosin contractility does not prevent cells from migrating. Instead, the "repulsive" effect of EPH/EPHRIN signaling in our system is one that regulates interfacial cortical tension to allow cells to minimize their heterotypic contacts while increasing homotypic EPHB2 contacts.

Nevertheless, it is possible that cell migration is playing a role in EPH/EPHRIN-driven cell segregation in other contexts in vivo where cells are confronted with dynamic and complex environments.

The results of our mouse genetics experiments are consistent with the requirement for cellular contractility in driving EPH/EPHRIN cellular self-organization; however, these experiments do not rule out the role of actomyosin in cell migration as a possible contributing mechanism as well. There is also the possibility that mechanisms of segregation may differ between cell types. Our study examines HEK293 cells and craniofacial mesenchyme cells. While HEK293 cells were thought to be epithelial in origin, HEK293 cells express a number of mesenchymal markers, such as N-cadherin and vimentin, and indeed have been speculated to have a neural crest-derived adrenal medulla origin (Inada et al., 2016; Lin et al., 2014). The effects of EPH/EPHRIN signaling on cortical tension and cell contacts will need to be examined in additional cell types that also form EPH/EPHRIN boundaries to determine the extent to which mechanisms differ between cell types.

Previous findings indicated that at the boundary between the mesoderm and ectoderm, tissue separation occurs due to EPHB forward signaling, and this separation occurs through repeated rounds of adhesion, which brings EPHs and EPHRINs into contact for active signaling, which then induces repulsion and detachment of the two tissues (Rohani et al., 2011). This is similar to our findings that cell:cell contacts are not static but, rather, dynamic over time. This detachment between the mesoderm and ectoderm could represent minimization of contact between germ layers driven by changing tension at the mesoderm–ectoderm interface. The analogy of EPH/EPHRIN signaling in segregation to its role in growth cone collapse may therefore better reflect the commonality of actomyosin contractility in cellular collapse and modulation of cell:cell contact rather than migratory guidance. Actomyosin contractility pathways are well established to be downstream of EPH/EPHRIN signaling and classically known to be involved in cellular collapse phenotypes induced by EPH/EPHRIN signaling (Wahl et al., 2000). The idea that EPH/EPHRIN signaling results in minimization of cell contacts by increased interfacial tension, therefore, may represent a broadly applicable mechanism by which EPHs and EPHRINs regulate cell behavior and boundary formation in morphogenesis.

It is notable that AFM revealed cortical stiffness increases in both EPHB2-expressing and EPHRIN-B1–expressing cells during segregation, whereas MLC fluorescence increases in EPHB2 cells at EPHB2:EPHRIN-B1 heterotypic contacts. Previous genetic experiments in *Efnb1* mutant mouse models indicated that unidirectional forward signaling drives EPH:EPHRIN cell segregation in the developing embryo, whereas reverse signaling is dispensable (O'Neill et al., 2016). Recent findings have shown that whereas polarized forward signaling is the principal driver of cell sorting, reverse signaling also plays a role in preventing cell intermingling, consistent with the increases in cortical stiffness that we observe in EPHRIN-B1 cells. This suggests a contribution of both forward and reverse signaling to EPH:EPHRIN cell segregation in cell culture, whereas forward signaling is sufficient in vivo, and the contributions of reverse signaling in vivo may be difficult to detect.

The data presented here suggest a novel model for EPH/EPHRIN-driven cell segregation in which both cell:cell and cell:medium tension, driven by actomyosin contractility, drive cellular organization and boundary formation. This expands our knowledge of boundary formation and suggests a generalizable mechanism by which EPH/EPHRIN signaling drives this morphogenetic process.

Materials and methods

HEK293 cell culture

Stable HEK293 cell lines expressing EPHRIN-B1 or EPHB2 plus membrane-targeted GFP were obtained from A. Poliakov and D. Wilkinson (laboratory of D. Wilkinson, Medical Research Council National Institute for Medical Research, London, UK; Poliakov et al., 2008; Jørgensen et al., 2009). Stable HEK293 cell lines expressing EPHB2, membrane-targeted GFP, and LifeAct-mCherry were generated as described in O'Neill et al. (2016). Stable HEK293 cell lines expressing EPHB2 or EPHRIN-B1 and MLC-cherry constructs were generated by transfecting EPHB2-GFP or EPHRIN-B1 cells with MLC-cherry plasmid DNA followed by selection with hygromycin. All cells were cultured at 37°C with 5% CO_2 in DMEM supplemented with 10% FBS, glutamine, and antibiotics. Serum starvation medium was made using DMEM with glutamine and antibiotics, and low-Ca^{2+} medium was made using spinner modification–minimum essential medium supplemented with 5% dialyzed FBS, glutamine, and antibiotics.

Cell segregation assay, static analysis of sorting, cell density quantification, and live imaging

Cell segregation assays were performed as previously described (Poliakov et al., 2008; O'Neill et al., 2016). Each cell type was aliquoted into and resuspended in medium to a cell density of 150,000/ml with various inhibitors and plated in 24-well plates coated with 10 µg/ml fibronectin (Sigma-Aldrich). For mixing experiments, HEK293 cells expressing GFP, LifeAct-mCherry, and high levels of EPHB2 (EPHB2-GFP-LifeAct-mCherry) were mixed with HEK293 cells expressing GFP and high levels of EPHB2 (EPHB2-GFP) as a control or with HEK293 cells expressing high levels of EPHRIN-B1 and LifeAct-mCherry (EPHRIN-B1-LifeAct-mCherry). Mixing of cells expressing EPHB2 with cells expressing EPHRIN-B1 resulted in dramatic segregation. Cells were mixed in a 1:1 ratio. For three cell type–mixing experiments, EPHB2-GFP-LifeAct-mCherry cells were mixed with EPHRIN-B1-LifeAct-mCherry and HEK293 cells expressing LifeAct-BFP (WT-LifeAct-BFP). Cells were then cultured for 24 or 48 h.

Images of live cells were acquired on an Axio Observer Z1 spinning disk confocal microscope (Zeiss) at 37° using a 10× objective lens. ZEN software was used to acquire images, adjust brightness and contract, and export Tag Image File Format images. For each condition, six to eight images were obtained per experimental replicate, and images were manually thresholded in ImageJ (Table S1). Experiments were repeated three to four times (Table S1). Segregation was then quantified using the nearest neighbor method (Mochizuki et al., 1998; Poliakov et al., 2008; O'Neill et al., 2016). This method converts each image into a lattice of squares, roughly corresponding to cells, and each square is scored as GFP^+ or GFP^-. For each GFP^+ square, the number of neighboring GFP^+ squares among the four nearest neighbors is counted, and this information generates a sorting score, as detailed in Mochizuki et al. (1998). Sorting scores were

normalized to the EPHB2-GFP + EPHB2-GFP-LifeAct-mCherry condition (negative control; set to 0.5), and raw data from images were averaged and analyzed using ANOVA and Dunnett's tests. All conditions were compared with the positive control condition (EPHB2-GFP-LifeAct-mCherry + EPHRIN-B1-LifeAct-mCherry + DMSO).

Cell density was quantified by adding Hoescht to cells at 24 or 48 h for 30 min before imaging. For each condition, six to eight images were obtained per experimental replicate, and images were manually thresholded in ImageJ (Table S1). Experiments were repeated three to four times (Table S1). In each image, the number of nuclei was counted using the cell counter in ImageJ. Nuclei were counted by cell type by using GFP to mark EPHB2 cells and absence of GFP for EPHRIN-B1 cells. GFP^+ area was then measured in ImageJ along with the total image area (in μm^2). Nuclei number was then divided by GFP^+ area for EPHB2 cells and GFP^- area for EPHRIN-B1 cells to obtain final cell density. For images with only one cell type, total nuclei number was divided by total image area.

For live imaging of cell segregation, EPHB2-GFP-LifeAct-mCherry and EPHRIN-B1-LifeAct-mCherry cells were mixed, at a 1:1 ratio, and plated in a glass bottom imaging dish coated with 10 µg/ml fibronectin (Sigma-Aldrich) to a final cell density of 400,000/ml. Mixing was performed in the presence of 20 µM Y27632 and 25 µM ML7 (EMD Millipore) or vehicle (0.25% DMSO). Live imaging began 1 h after plating and was performed at 37°C. Hepes buffer (15 mM) was added and the dish sealed to buffer CO_2. Confocal stacks (3 × 2 µm) were acquired every 10 min for 16 h using an Axio Observer Z1 spinning disk confocal microscope (Zeiss) at 37°C, a 40× water LD C-Apochromat objective lens (NA 1.1; Zeiss), and an Axiocam 506 camera (Zeiss). ZEN software was used to acquire images and generate maximum intensity projections. Three videos were acquired, and cell tracking analysis was performed using the Manual Tracking plugin in ImageJ. Cells that could not be tracked for at least 12 consecutive frames (2 h in real time) were excluded from the analysis (Table S1). For statistical analysis, ANOVAs (with Dunnett's post hoc tests) were used.

For low-density live imaging of cell contacts, cells were plated in a glass bottom imaging dish coated with 10 µg/ml fibronectin to a final cell density of 60,000/ml. In mixed EPHRIN-B1-MLC-cherry + EPHB2-GFP-MLC-cherry cultures, EPHRIN-B1 cells were plated 30 min before plating EPHB2 cells. In control EPHRIN-B1-MLC-cherry conditions, half of the total EPHRIN-B1 cells were plated 30 min before plating the second half of the EPHRIN-B1 cells, and in control EPHB2 conditions, EPHB2-GFP cells were plated first followed by EPHB2-GFP-MLC-cherry cells. Live imaging began 15 min after plating the second cell population and was performed at 37°C. Hepes buffer (15 mM) was added and the dish sealed to buffer CO_2. Confocal stacks (3 × 2 µm) were acquired every 3 min for 8 h using an Axio Observer Z1 spinning disk confocal microscope (Zeiss) at 37°C, a 40× water LD C-Apochromat objective lens (NA 1.1; Zeiss), and an Axiocam 506 camera (Zeiss). ZEN software was used to acquire images. Line scan analysis was performed on a single Z-position using ImageJ, with line scans being drawn approximately perpendicular to the cell:cell contact. We chose cell pairs where we believed we were analyzing the first heterotypic cell:cell interaction. The change in MLC fluorescence was calculated by taking the highest value from the line scan at the membrane toward the cell:cell contact both before contact (t = −15 min) and after contact (t = 30 min). The value before contact was subtracted from the value after contact to determine the change in MLC fluorescence at the cell:cell contact. Five cell pairs were analyzed for each condition.

Fabrication of agarose microwells, cell:cell contact angle and circular microwell hierarchy assays, and cell:cell live imaging

Agarose microwells were prepared as described in Cerchiari et al. (2015). Briefly, photomasks containing the desired features (a grid of 20 × 40–µm oblongs or 180-µm circles) were obtained from CAD/Art Services, Inc. Silicon wafers were spin-coated with a 50-µm-thick layer of SU-8 photoresist and baked at 135°C for 10 min. The photomask was positioned above the wafer and irradiated with UV light for 2 min. The wafer was placed in SU-8 developer for 10 min after 1 min postexposure bake at 135°C. After development, the wafer was rinsed twice with SU-8 developer and once with isopropanol and baked at 135°C for 5 min. SYLGARD 184 silicone elastomer was prepared as per the manufacturer's instructions and poured over the developed wafer. Any air bubbles present were removed by placing in a desiccator for 15–30 min. The PDMS was cured at 60°C overnight. Stamps were made by removing the PDMS from the wafer and cutting PDMS into 1 cm × 1 cm pieces. To make the microwells, a PDMS stamp was gently placed on top of molten 2% agarose in PBS within a two-well chambered coverglass. The PDMS stamp was carefully lifted once the agarose solidified.

Cell:cell contact angle assay was performed similarly to that previously described in Cerchiari et al. (2015). Unmixed or mixed populations of cells were centrifuged into agarose microwells at 200 *g* for 6 min at a concentration of 10^6/ml. Excess cells were then washed away with culture medium, and the remaining cells confined in wells were incubated for 4–12 h for two-cell pairs and 24–48 h for circular microwells. Cell pairs were imaged 4 h after plating using an Axio Observer Z1 spinning disk confocal microscope (Zeiss) at 37°C with a 40× water LD C-Apochromat objective lens (NA 1.1; Zeiss). Cell aggregates were imaged immediately after plating (0 h), as well as at 24 and 48 h. ZEN software was used to acquire images, adjust brightness and contrast, and export Tag Image File Format images. Contact angles were measured manually using the ImageJ tool for angle measurement. For each cell doublet, angles M_1–M_4 were measured and subtracted from 180 to obtain Θ (Fig. 1 A). These four Θ values were then averaged to generate one contact angle measurement per cell doublet and plotted as contact angles. Between 54 and 205 cell doublets were measured per condition across 3–10 replicates (Table S1). Raw data from images were analyzed using ANOVA and Dunnett's tests.

For live imaging of cell:cell contact, 2% agarose in PBS microwells was made within a glass bottom imaging dish and incubated in cell culture media for 24 h. EPHB2-GFP-LifeAct-mCherry and EPHRIN-B1-LifeAct-mCherry cells were mixed, or plated without being mixed, into microwells and centrifuged into agarose microwells at 200 *g* for 6 min. Excess cells were

then washed away, and 15 mM Hepes buffer was added and the dish sealed. Imaging began 30 min after plating and was performed at 37°C. Confocal stacks (5 × 2 µm) were acquired every 5 min for 12 h using an Axio Observer Z1 spinning disk confocal microscope (Zeiss) at 37°C, a 40× water LD C-Apochromat objective lens (NA 1.1; Zeiss), and an Axiocam 506 camera (Zeiss). ZEN software was used to acquire images and generate maximum intensity projections.

Hanging drop assays

EPHB2-GFP-LifeAct-mCherry cells were mixed with either EPHB2-GFP (control), or EPHRIN-B1-LifeAct-mCherry (cell segregation conditions). Cells were mixed in a 1:1 ratio for a total of 10^6 cells/ml. Ten microliter drops of cell suspension were plated on the lid of a 10-cm dish and inverted for culture. Medium was put into the dish to maintain humidity. For large hanging drops, cultures were incubated for 72 h and imaged for controls or 96 and 120 h with the addition of inhibitors at 72 h. For isolated hanging drops, small aggregates that form by 24 h of culture were manually isolated using a dissecting microscope to visualize individual aggregates. Individual aggregates were then plated in 10-µl drops on the lid of a 10-cm dish and inverted for culture. Aggregate isolation and replating was performed in the presence of 20 µM Y27632 and 25 µM ML7 or DMSO. Isolated aggregates were then cultured for an additional 48 h. Hanging drops were imaged by transferring single drops onto a glass bottom dish for imaging. Images were acquired using an Axio Observer Z1 spinning disk confocal microscope (Zeiss) at 37°C at 10× and an Axiocam 506 camera (Zeiss). ZEN software was used to acquire images and generate maximum intensity projections.

AFM

EPHB2-GFP and EPHRIN-B1-LifeAct-mCherry cells were serum starved for 48 h in order to synchronize cell cycle. After 48 h of serum starvation, cells were switched back into regular culture media for 24 h before mixing. EPHB2-GFP and EPHRIN-B1-LifeAct-mCherry cells were either mixed and plated or plated alone onto glass coverslips coated with 10 µg/ml fibronectin (Sigma-Aldrich) to a final cell density of 400,000/ml. For inhibitor experiments, Y27632 and ML7, or DMSO for controls, were added at the time of cell mixing. AFM was performed 2, 4, or 24 h after mixing. For inhibitor experiments and 2- and 4-h analysis, data were collected across EPHB2 and EPHRIN-B1 cell types and presented as pooled data, while at 24 h, EPHB2 and EPHRIN-B1 populations were measured separately in mixed conditions. Glass coverslips were placed on slides and placed on the stage of an MFP3D-BIO inverted optical AFM (Asylum Research) mounted on a Nikon TE2000-U inverted microscope. Indentations were made using silicon nitride cantilevers with spring constants ranging from 0.05 to 0.07 N/m and modified with borosilicate glass spherical tips 5 µm in diameter (Novascan Technologies). The cantilevers were calibrated using the thermal oscillation method before each experiment. Cells were indented at rates ranging from 0.75 to 1.5 µm/s and with a maximum force of 4.5 nN. The Hertz model was applied to the force curves obtained from each cell indentation to calculate the elastic modulus (Young's modulus, stiffness). Cells were assumed to be incompressible; therefore, a Poisson ratio of 0.5 was used in the calculation of the elastic modulus. Experiments were repeated three to six times per condition (Table S1). Raw data were analyzed using ANOVA and Dunnett's tests.

Inhibitors

Inhibitors used in cell segregation assays, cell:cell contact angle assays, and live imaging were 2 µg/ml unclustered EPHRIN-B1-Fc (R&D Systems), 20 µM Y27632 (Cayman Chemical), 25 µM ML7 (EMD Millipore), 20 µM blebbistatin (Sigma-Aldrich), and 5 µg/ml mitomycin C (Sigma-Aldrich).

Mouse lines

All alleles used here have been previously described. All mice were maintained on a congenic C57BL/6J genetic background. Efnb1lox (MGI: 3039289; Davy et al., 2004); XGFP (Mouse Genome Informatics [MGI] under accession no. MGI:3055027; Hadjantonakis et al., 1998), Shox2IresCre (MGI under accession no. MGI:5567920; Dougherty et al., 2013), NMIIA$^{lox/lox}$ (MGI under accession no. MGI:4838521; Jacobelli et al., 2010), and NMIIB$^{lox/lox}$ (MGI under accession no. MGI:4443039; Ma et al., 2009; Table S2). To ensure X chromosome mosaicism, all embryos were female and collected at embryonic day 13.5.

Immunofluorescence

Embryos were fixed in 4% PFA in PBS, dehydrated through sucrose, embedded in optimum cutting temperature compound, and frozen in dry ice/ethanol. Ten-micrometer sections were cut using a CryoStar NX70 Cryostat (Thermo Scientific). Slides were washed with PBS, blocked in 5% normal donkey serum (Jackson ImmunoResearch) and 0.1% Triton X-100 in PBS, incubated in primary antibody overnight at 4°C, washed with PBS, and incubated in secondary antibody at room temperature. Slides were counterstained in DAPI (Millipore) in PBS, and coverslips were mounted on slides using Aqua-Mount (Thermo Scientific) for imaging. Images were acquired on an LSM 900 confocal laser scanning microscope (Zeiss) on an LD LCI Plan-Apochromat 25×/0.8 Imm Corr DIC M27 objective lens. ZEN software was used to acquire images and generate maximum intensity projections.

Quantification of cell segregation in vivo

Quantification of cell segregation in vivo was performed on cryosections immunostained for EPHRIN-B1 and XGFP, and counterstained with DAPI. For quantification, continuous XGFP-expressing regions were selected in FIJI/ImageJ, and area was calculated as a measure of the amount of cell segregation. Additionally, the total number of nuclei in each XGFP$^+$ patch was counted manually, using the cell counter plug-in. XGFP$^+$ patches were binned into patches sizes of 1–5, 6–64, 65–128, >128 nuclei, and the number of patches in each bin was divided by the total number of XGFP$^+$ patches in that section to generate the percentage of patches of different size ranges. Images from three different embryos of each genotype were analyzed (Table S1 and Table S3).

Online supplemental material

Table S1 shows sample size and replicate numbers for all quantified experiments, Table S2 contains genetic crosses used

to generate experimental and control mouse embryos, and Table S3 shows the number of embryos analyzed. Videos 1, 2, 3, and 4 show live imaging of cell pairs in agarose microwells over 12 h. Videos 5, 6, 7, 8, 9, 10, 11, and 12 show live imaging of MLC-Cherry cell lines, showing an increase in MLC localization in EPHB2 cells upon heterotypic contact. Fig. S1 shows that heterotypic EPHB2:EPHRIN-B1 cells maintain high interfacial tension over time, and heterotypic HEK293 cell pairs that do not have active EPH/EPHRIN signaling do not have increased interfacial tension, similar to homotypic cell pairs. Fig. S2 shows that cells under dual inhibition of ROCK and MLCK inhibitors are as migratory as cells undergoing active cell segregation and that mitomycin C treatment does not disrupt cell segregation. Fig. S3 shows that cells show an increase cortical tension before segregation, and inhibition of contractility decreases stiffness of cells in mixed cultures. Fig. S4 shows that MLC localization increases at heterotypic contacts. Fig. S5 shows that EPHB2 cells increase their homotypic contacts as a result of EPH/EPHRIN signaling. Fig. S6 shows that EPH/EPHRIN signaling affects cortical tension tissue morphology.

Acknowledgments

The authors thank Matt Kutys for advice concerning MLC localization experiments. We thank Matt Kutys and Diane Barber for critical reading of the manuscript.

This work was supported by National Institutes of Health/National Institute of Dental and Craniofacial Research grant R01DE023337 and National Institutes of Health/National Heart, Lung, and Blood Institute grant R01HL144785 to J.O. Bush. A.A. Kindberg was supported by National Institutes of Health/National Institute of Dental and Craniofacial Research Ruth L. Kirschstein Predoctoral National Research Service Award F31DE028175.

The authors declare no competing financial interests.

Author contributions: A.A. Kindberg and J.O. Bush conceived the project and conceptualized the experiments. A.A. Kindberg performed most of the experiments, aided by V. Srivastava and J.M. Muncie. V. Srivastava assisted with initial microwell experiments and generated PDMS stamps for microwell studies. J.M. Muncie performed AFM experiments and analyzed AFM data. A.A. Kindberg analyzed all other data. V.M. Weaver and Z.J. Gartner provided intellectual input and resources. A.A. Kindberg and J.O. Bush wrote the manuscript and received manuscript review and editing from V. Srivastava, J.M. Muncie, V.M. Weaver, and Z.J. Gartner.

Submitted: 12 June 2020
Revised: 2 February 2021
Accepted: 3 March 2021

References

Astin, J.W., J. Batson, S. Kadir, J. Charlet, R.A. Persad, D. Gillatt, J.D. Oxley, and C.D. Nobes. 2010. Competition amongst Eph receptors regulates contact inhibition of locomotion and invasiveness in prostate cancer cells. *Nat. Cell Biol.* 12:1194–1204. https://doi.org/10.1038/ncb2122

Batlle, E., and D.G. Wilkinson. 2012. Molecular mechanisms of cell segregation and boundary formation in development and tumorigenesis. *Cold Spring Harb. Perspect. Biol.* 4:a008227. https://doi.org/10.1101/cshperspect.a008227

Batlle, E., J.T. Henderson, H. Beghtel, M.M.W. van den Born, E. Sancho, G. Huls, J. Meeldijk, J. Robertson, M. van de Wetering, T. Pawson, and H. Clevers. 2002. β-catenin and TCF mediate cell positioning in the intestinal epithelium by controlling the expression of EphB/ephrinB. *Cell.* 111:251–263. https://doi.org/10.1016/S0092-8674(02)01015-2

Bhagavathula, N., A.W. Hanosh, K.C. Nerusu, H. Appelman, S. Chakrabarty, and J. Varani. 2007. Regulation of E-cadherin and β-catenin by Ca2+ in colon carcinoma is dependent on calcium-sensing receptor expression and function. *Int. J. Cancer.* 121:1455–1462. https://doi.org/10.1002/ijc.22858

Brasch, J., O.J. Harrison, B. Honig, and L. Shapiro. 2012. Thinking outside the cell: how cadherins drive adhesion. *Trends Cell Biol.* 22:299–310. https://doi.org/10.1016/j.tcb.2012.03.004

Brodland, G.W. 2002. The Differential Interfacial Tension Hypothesis (DITH): a comprehensive theory for the self-rearrangement of embryonic cells and tissues. *J. Biomech. Eng.* 124:188–197. https://doi.org/10.1115/1.1449491

Brodland, G.W., and H.H. Chen. 2000. The mechanics of cell sorting and envelopment. *J. Biomech.* 33:845–851. https://doi.org/10.1016/S0021-9290(00)00011-7

Bush, J.O., and P. Soriano. 2010. Ephrin-B1 forward signaling regulates craniofacial morphogenesis by controlling cell proliferation across Eph-ephrin boundaries. *Genes Dev.* 24:2068–2080. https://doi.org/10.1101/gad.1963210

Calzolari, S., J. Terriente, and C. Pujades. 2014. Cell segregation in the vertebrate hindbrain relies on actomyosin cables located at the interhombomeric boundaries. *EMBO J.* 33:686–701. https://doi.org/10.1002/embj.201386003

Canty, L., E. Zarour, L. Kashkooli, P. François, and F. Fagotto. 2017. Sorting at embryonic boundaries requires high heterotypic interfacial tension. *Nat. Commun.* 8:157. https://doi.org/10.1038/s41467-017-00146-x

Cayuso, J., Q. Xu, M. Addison, and D.G. Wilkinson. 2019. Actomyosin regulation by Eph receptor signaling couples boundary cell formation to border sharpness. *eLife.* 8:e49696. https://doi.org/10.7554/eLife.49696

Cerchiari, A.E., J.C. Garbe, N.Y. Jee, M.E. Todhunter, K.E. Broaders, D.M. Peehl, T.A. Desai, M.A. LaBarge, M. Thomson, and Z.J. Gartner. 2015. A strategy for tissue self-organization that is robust to cellular heterogeneity and plasticity. *Proc. Natl. Acad. Sci. USA.* 112:2287–2292. https://doi.org/10.1073/pnas.1410776112

Compagni, A., M. Logan, R. Klein, and R.H. Adams. 2003. Control of skeletal patterning by ephrinB1-EphB interactions. *Dev. Cell.* 5:217–230. https://doi.org/10.1016/S1534-5807(03)00198-9

Cooke, J., C. Moens, L. Roth, L. Durbin, K. Shiomi, C. Brennan, C. Kimmel, S. Wilson, and N. Holder. 2001. Eph signalling functions downstream of Val to regulate cell sorting and boundary formation in the caudal hindbrain. *Development.* 128:571–580.

Davy, A., J. Aubin, and P. Soriano. 2004. Ephrin-B1 forward and reverse signaling are required during mouse development. *Genes Dev.* 18:572–583. https://doi.org/10.1101/gad.1171704

Dougherty, K.J., L. Zagoraiou, D. Satoh, I. Rozani, S. Doobar, S. Arber, T.M. Jessell, and O. Kiehn. 2013. Locomotor rhythm generation linked to the output of spinal shox2 excitatory interneurons. *Neuron.* 80:920–933. https://doi.org/10.1016/j.neuron.2013.08.015

Duguay, D., R.A. Foty, and M.S. Steinberg. 2003. Cadherin-mediated cell adhesion and tissue segregation: qualitative and quantitative determinants. *Dev. Biol.* 253:309–323. https://doi.org/10.1016/S0012-1606(02)00016-7

Fagotto, F. 2014. The cellular basis of tissue separation. *Development.* 141:3303–3318. https://doi.org/10.1242/dev.090332

Foty, R.A., and M.S. Steinberg. 2005. The differential adhesion hypothesis: a direct evaluation. *Dev. Biol.* 278:255–263. https://doi.org/10.1016/j.ydbio.2004.11.012

Gale, N.W., S.J. Holland, D.M. Valenzuela, A. Flenniken, L. Pan, T.E. Ryan, M. Henkemeyer, K. Strebhardt, H. Hirai, D.G. Wilkinson, et al. 1996. Eph receptors and ligands comprise two major specificity subclasses and are reciprocally compartmentalized during embryogenesis. *Neuron.* 17:9–19. https://doi.org/10.1016/S0896-6273(00)80276-7

Hadjantonakis, A.-K., M. Gertsenstein, M. Ikawa, M. Okabe, and A. Nagy. 1998. Non-invasive sexing of preimplantation stage mammalian embryos. *Nat. Genet.* 19:220–222. https://doi.org/10.1038/893

Harris, A.K. 1976. Is cell sorting caused by differences in the work of intercellular adhesion? A critique of the Steinberg hypothesis. *J. Theor. Biol.* 61:267–285. https://doi.org/10.1016/0022-5193(76)90019-9

Inada, M., G. Izawa, W. Kobayashi, and M. Ozawa. 2016. 293 cells express both epithelial as well as mesenchymal cell adhesion molecules. *Int. J. Mol. Med.* 37:1521–1527. https://doi.org/10.3892/ijmm.2016.2568

Jacobelli, J., R.S. Friedman, M.A. Conti, A.-M. Lennon-Dumenil, M. Piel, C.M. Sorensen, R.S. Adelstein, and M.F. Krummel. 2010. Confinement-optimized three-dimensional T cell amoeboid motility is modulated via myosin IIA-regulated adhesions. *Nat. Immunol.* 11:953–961. https://doi.org/10.1038/ni.1936

Jørgensen, C., A. Sherman, G.I. Chen, A. Pasculescu, A. Poliakov, M. Hsiung, B. Larsen, D.G. Wilkinson, R. Linding, and T. Pawson. 2009. Cell-specific information processing in segregating populations of Eph receptor ephrin-expressing cells. *Science.* 326:1502–1509. https://doi.org/10.1126/science.1176615

Kindberg, A.A., and J.O. Bush. 2019. Cellular organization and boundary formation in craniofacial development. *Genesis.* 57:e23271. https://doi.org/10.1002/dvg.23271

Krieg, M., Y. Arboleda-Estudillo, P.-H. Puech, J. Käfer, F. Graner, D.J. Müller, and C.-P. Heisenberg. 2008. Tensile forces govern germ-layer organization in zebrafish. *Nat. Cell Biol.* 10:429–436. https://doi.org/10.1038/ncb1705

Kullander, K., and R. Klein. 2002. Mechanisms and functions of Eph and ephrin signalling. *Nat. Rev. Mol. Cell Biol.* 3:475–486. https://doi.org/10.1038/nrm856

Lecuit, T., and P.-F. Lenne. 2007. Cell surface mechanics and the control of cell shape, tissue patterns and morphogenesis. *Nat. Rev. Mol. Cell Biol.* 8:633–644. https://doi.org/10.1038/nrm2222

Lecuit, T., and A.S. Yap. 2015. E-cadherin junctions as active mechanical integrators in tissue dynamics. *Nat. Cell Biol.* 17:533–539. https://doi.org/10.1038/ncb3136

Lin, Y.-C., M. Boone, L. Meuris, I. Lemmens, N. Van Roy, A. Soete, J. Reumers, M. Moisse, S. Plaisance, R. Drmanac, et al. 2014. Genome dynamics of the human embryonic kidney 293 lineage in response to cell biology manipulations. *Nat. Commun.* 5:4767. https://doi.org/10.1038/ncomms5767

Ma, X., K. Takeda, A. Singh, Z.-X. Yu, P. Zerfas, A. Blount, C. Liu, J.A. Towbin, M.D. Schneider, R.S. Adelstein, and Q. Wei. 2009. Conditional ablation of nonmuscle myosin II-B delineates heart defects in adult mice. *Circ. Res.* 105:1102–1109. https://doi.org/10.1161/CIRCRESAHA.109.200303

Maître, J.-L., and C.-P. Heisenberg. 2013. Three functions of cadherins in cell adhesion. *Curr. Biol.* 23:R626–R633. https://doi.org/10.1016/j.cub.2013.06.019

Maître, J.-L., H. Berthoumieux, S.F.G. Krens, G. Salbreux, F. Jülicher, E. Paluch, and C.-P. Heisenberg. 2012. Adhesion functions in cell sorting by mechanically coupling the cortices of adhering cells. *Science.* 338:253–256. https://doi.org/10.1126/science.1225399

Mellitzer, G., Q. Xu, and D.G. Wilkinson. 1999. Eph receptors and ephrins restrict cell intermingling and communication. *Nature.* 400:77–81. https://doi.org/10.1038/21907

Merrill, A.E., E.G. Bochukova, S.M. Brugger, M. Ishii, D.T. Pilz, S.A. Wall, K.M. Lyons, A.O.M. Wilkie, and R.E. Maxson Jr. 2006. Cell mixing at a neural crest-mesoderm boundary and deficient ephrin-Eph signaling in the pathogenesis of craniosynostosis. *Hum. Mol. Genet.* 15:1319–1328. https://doi.org/10.1093/hmg/ddl052

Mochizuki, A., N. Wada, H. Ide, and Y. Iwasa. 1998. Cell-cell adhesion in limb-formation, estimated from photographs of cell sorting experiments based on a spatial stochastic model. *Dev. Dyn.* 211:204–214. https://doi.org/10.1002/(SICI)1097-0177(199803)211:3<204::AID-AJA2>3.0.CO;2-L

Niethamer, T.K., and J.O. Bush. 2019. Getting direction(s): the Eph/ephrin signaling system in cell positioning. *Dev. Biol.* 447:42–57. https://doi.org/10.1016/j.ydbio.2018.01.012

Niethamer, T.K., A.R. Larson, A.K. O'Neill, M. Bershteyn, E.C. Hsiao, O.D. Klein, J.H. Pomerantz, and J.O. Bush. 2017. EPHRIN-B1 mosaicism drives cell segregation in craniofrontonasal syndrome hiPSC-derived neuroepithelial cells. *Stem Cell Reports.* 8:529–537. https://doi.org/10.1016/j.stemcr.2017.01.017

Niethamer, T.K., T. Teng, M. Franco, Y.X. Du, C.J. Percival, and J.O. Bush. 2020. Aberrant cell segregation in the craniofacial primordium and the emergence of facial dysmorphology in craniofrontonasal syndrome. *PLoS Genet.* 16:e1008300. https://doi.org/10.1371/journal.pgen.1008300

O'Neill, A.K., A.A. Kindberg, T.K. Niethamer, A.R. Larson, H.H. Ho, M.E. Greenberg, and J.O. Bush. 2016. Unidirectional Eph/ephrin signaling creates a cortical actomyosin differential to drive cell segregation. *J. Cell Biol.* 215:217–229. https://doi.org/10.1083/jcb.201604097

Pasquale, E.B. 2010. Eph receptors and ephrins in cancer: bidirectional signalling and beyond. *Nat. Rev. Cancer.* 10:165–180. https://doi.org/10.1038/nrc2806

Poliakov, A., M.L. Cotrina, A. Pasini, and D.G. Wilkinson. 2008. Regulation of EphB2 activation and cell repulsion by feedback control of the MAPK pathway. *J. Cell Biol.* 183:933–947. https://doi.org/10.1083/jcb.200807151

Porazinski, S., J. de Navascués, Y. Yako, W. Hill, M.R. Jones, R. Maddison, Y. Fujita, and C. Hogan. 2016. EphA2 drives the segregation of Ras-transformed epithelial cells from normal neighbors. *Curr. Biol.* 26:3220–3229. https://doi.org/10.1016/j.cub.2016.09.037

Rodríguez-Franco, P., A. Brugués, A. Marín-Llauradó, V. Conte, G. Solanas, E. Batlle, J.J. Fredberg, P. Roca-Cusachs, R. Sunyer, and X. Trepat. 2017. Long-lived force patterns and deformation waves at repulsive epithelial boundaries. *Nat. Mater.* 16:1029–1037. https://doi.org/10.1038/nmat4972

Rohani, N., L. Canty, O. Luu, F. Fagotto, and R. Winklbauer. 2011. EphrinB/EphB signaling controls embryonic germ layer separation by contact-induced cell detachment. *PLoS Biol.* 9:e1000597. https://doi.org/10.1371/journal.pbio.1000597

Slováková, J., M. Sikora, S. Caballero-Mancebo, S.F.G. Krens, W.A. Kaufmann, K. Huljev, and C.-P. Heisenberg. 2020. Tension-dependent stabilization of E-cadherin limits cell-cell contact expansion. *bioRxiv.* 2020.11.20.391284. doi:. https://doi.org/10.1101/2020.11.20.391284

Solanas, G., C. Cortina, M. Sevillano, and E. Batlle. 2011. Cleavage of E-cadherin by ADAM10 mediates epithelial cell sorting downstream of EphB signalling. *Nat. Cell Biol.* 13:1100–1107. https://doi.org/10.1038/ncb2298

Steinberg, M.S. 1963. Reconstruction of tissues by dissociated cells. Some morphogenetic tissue movements and the sorting out of embryonic cells may have a common explanation. *Science.* 141:401–408. https://doi.org/10.1126/science.141.3579.401

Steinberg, M.S., and M. Takeichi. 1994. Experimental specification of cell sorting, tissue spreading, and specific spatial patterning by quantitative differences in cadherin expression. *Proc. Natl. Acad. Sci. USA.* 91:206–209. https://doi.org/10.1073/pnas.91.1.206

Stirbat, T.V., A. Mgharbel, S. Bodennec, K. Ferri, H.C. Mertani, J.-P. Rieu, and H. Delanoë-Ayari. 2013. Fine tuning of tissues' viscosity and surface tension through contractility suggests a new role for α-catenin. *PLoS One.* 8:e52554. https://doi.org/10.1371/journal.pone.0052554

Taylor, H.B., A. Khuong, Z. Wu, Q. Xu, R. Morley, L. Gregory, A. Poliakov, W.R. Taylor, and D.G. Wilkinson. 2017. Cell segregation and border sharpening by Eph receptor-ephrin-mediated heterotypic repulsion. *J. R. Soc. Interface.* 14:20170338. https://doi.org/10.1098/rsif.2017.0338

Ting, M.-C., N.L. Wu, P.G. Roybal, J. Sun, L. Liu, Y. Yen, and R.E. Maxson Jr. 2009. EphA4 as an effector of Twist1 in the guidance of osteogenic precursor cells during calvarial bone growth and in craniosynostosis. *Development.* 136:855–864. https://doi.org/10.1242/dev.028605

Twigg, S.R.F., R. Kan, C. Babbs, E.G. Bochukova, S.P. Robertson, S.A. Wall, G.M. Morriss-Kay, and A.O.M. Wilkie. 2004. Mutations of ephrin-B1 (EFNB1), a marker of tissue boundary formation, cause craniofrontonasal syndrome. *Proc. Natl. Acad. Sci. USA.* 101:8652–8657. https://doi.org/10.1073/pnas.0402819101

Wahl, S., H. Barth, T. Ciossek, K. Aktories, and B.K. Mueller. 2000. Ephrin-A5 induces collapse of growth cones by activating Rho and Rho kinase. *J. Cell Biol.* 149:263–270. https://doi.org/10.1083/jcb.149.2.263

Watanabe, T., Y. Sato, D. Saito, R. Tadokoro, and Y. Takahashi. 2009. EphrinB2 coordinates the formation of a morphological boundary and cell epithelialization during somite segmentation. *Proc. Natl. Acad. Sci. USA.* 106:7467–7472. https://doi.org/10.1073/pnas.0902859106

Winklbauer, R. 2015. Cell adhesion strength from cortical tension - an integration of concepts. *J. Cell Sci.* 128:3687–3693. https://doi.org/10.1242/jcs.174623

Wu, Z., T.G. Ashlin, Q. Xu, and D.G. Wilkinson. 2019. Role of forward and reverse signaling in Eph receptor and ephrin mediated cell segregation. *Exp. Cell Res.* 381:57–65. https://doi.org/10.1016/j.yexcr.2019.04.040

Yi, C., S. Troutman, D. Fera, A. Stemmer-Rachamimov, J.L. Avila, N. Christian, N.L. Persson, A. Shimono, D.W. Speicher, R. Marmorstein, et al. 2011. A tight junction-associated Merlin-angiomotin complex mediates Merlin's regulation of mitogenic signaling and tumor suppressive functions. *Cancer Cell.* 19:527–540. https://doi.org/10.1016/j.ccr.2011.02.017

Supplemental material

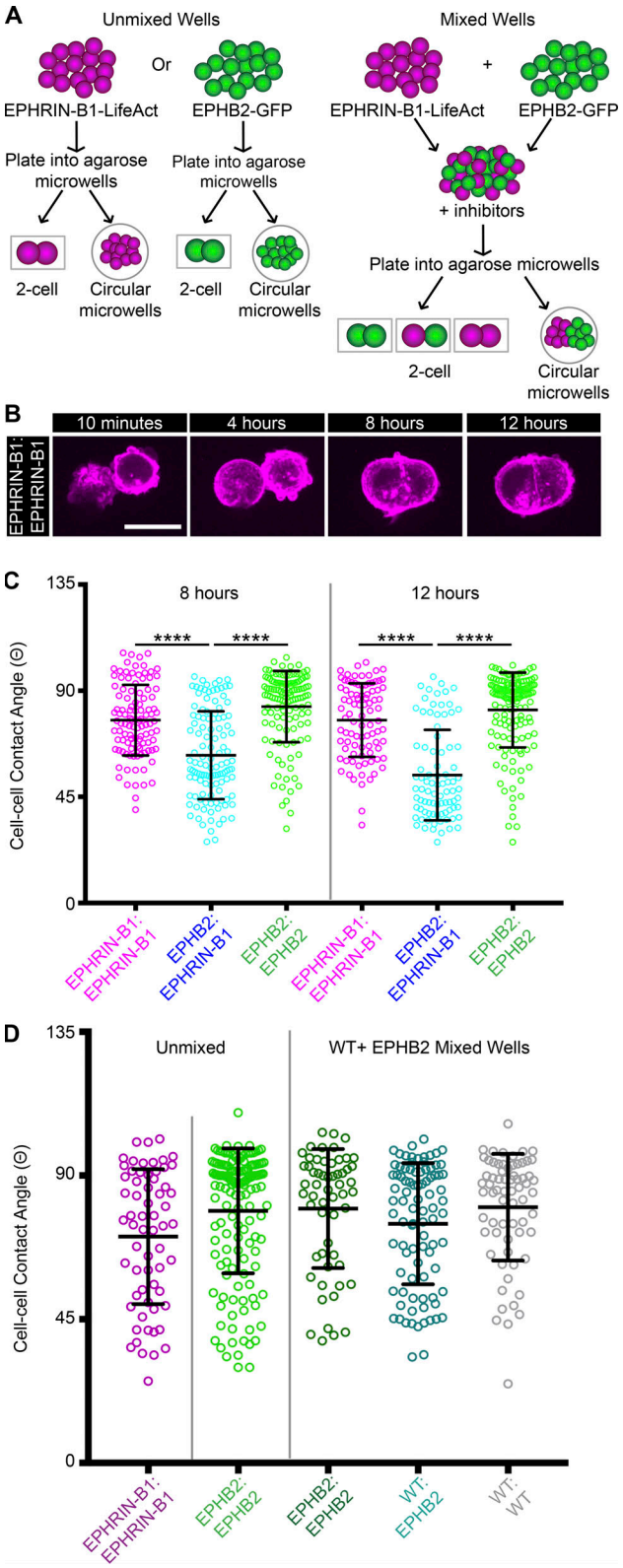

Figure S1. **HEK293 cells lacking EPH/EPHRIN signaling do not have high interfacial tension. (A)** Schematic of cell:cell contact angle assay set up for both unmixed and mixed conditions. **(B)** Individual frames from live imaging (Video 4) at 10 min, 4 h, 8 h, and 12 h of live imaging, showing that cell:cell contacts are dynamic over time. Scale bar, 20 µm. **(C)** Quantification of cell:cell contact angles at 8 h and 12 h after plating. EPHB2:EPHRIN-B1 cell pairs show a decreased contact angle, or increased interfacial tension, over time. **(D)** Quantification of cell:cell contact angles at 4 h after plating for unmixed EPHRIN-B1, unmixed EPHB2 cells, and mixed EPHB2 cells with WT HEK293 cells, showing that heterotypic cell pairs where no EPH/EPHRIN signaling is occurring do not display increased interfacial tension compared with homotypic cells. Error bars represent mean ± SD. ****, $P < 0.0001$ (ANOVA followed by Dunnett's multiple comparison test).

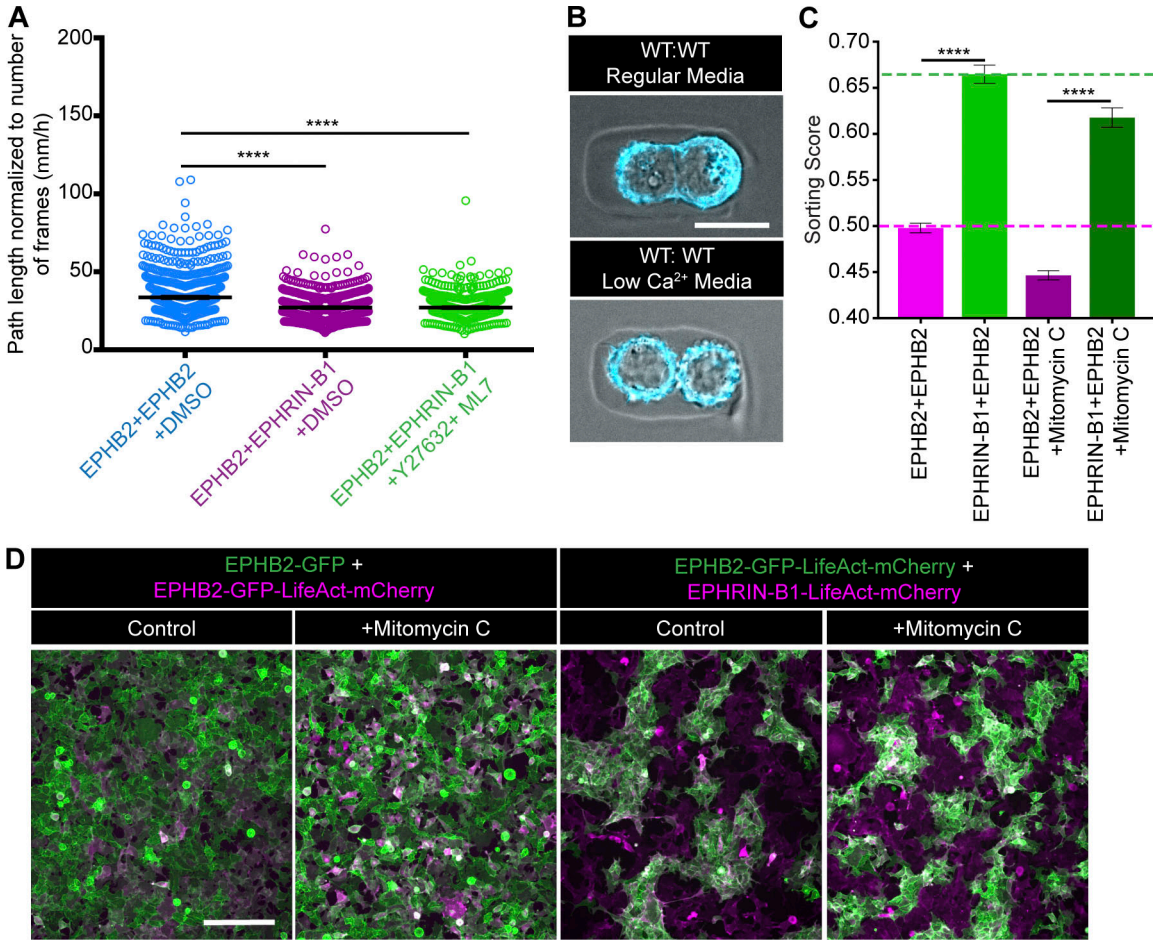

Figure S2. **Cells under dual ROCK and MLCK inhibition remain motile. (A)** Cell tracking analysis of overall EPHB2 cell movement over 16 h. EPHB2 cells in segregation conditions migrate less than when mixed with other EPHB2-expressing cells; however, addition of Y27632 and ML7 does not diminish migration from what is seen in cell segregation conditions. Error bars represent mean ± SEM. **(B)** Representative images of WT HEK293 cells in regular media and in low-Ca^{2+} media. Cell contact is dramatically reduced in the absence of calcium. Scale bar, 20 µm. **(C)** Quantification of cell segregation in the presence of mitomycin C. Inhibition of cellular proliferation does not block cell segregation. Column heights represent means of the technical replicates, and error bars represent SEM. **(D)** Representative images of cell segregation in mixed population of HEK293 cells in the presence of mitomycin C inhibitor. Scale bar, 200 µm. ****, $P < 0.0001$.

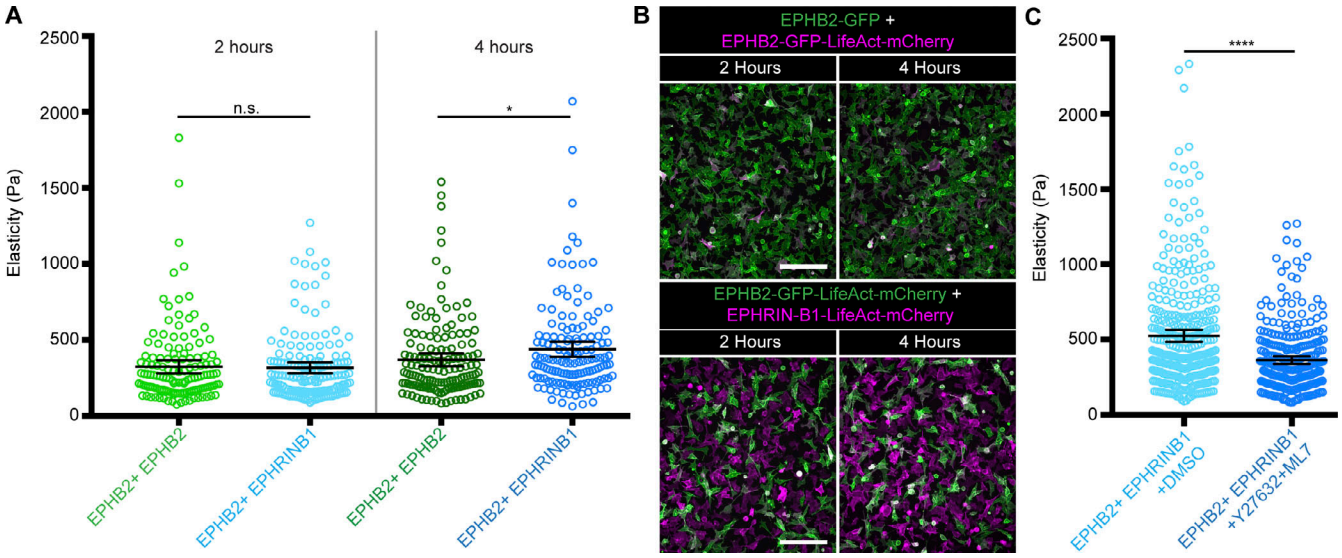

Figure S3. **Actomyosin contractility increases cortical tension during cell segregation at early time points. (A)** Quantification of cellular elasticity (Pa) determined by AFM in mixed EPHB2 cells cultured alone and EPHRIN-B1:EPHB2 mixed cultures at 2 and 4 h after plating. By 4 h after plating, EPHB2:EPHRIN-B1 mixed cultures show increased stiffness compared with EPHB2 cells cultured alone. *, $P < 0.05$. **(B)** Representative images of EPHB2-GFP-LifeAct-mCherry (magenta) cells mixed with EPHB2-GFP (green) cells mixed or EPHRIN-B1- LifeAct-mCherry (magenta) cells at 2 h and 4 h when AFM was performed. Cells in EPH:EPHRIN mixed cultures are not yet segregated. Scale bars, 200 µm. **(C)** Quantification of cellular elasticity (Pa) determined by AFM in mixed EPHRIN-B1: EPHB2 cultures in the presence of DMSO or actomyosin contractility inhibitors Y27632 and ML7 after 24 h. In the presence of contractility inhibitors, cells show a decrease in stiffness compared with DMSO controls. Error bars represent mean with 95% CI. ****, $P < 0.0001$ (ANOVA followed by Dunnett's multiple comparison test).

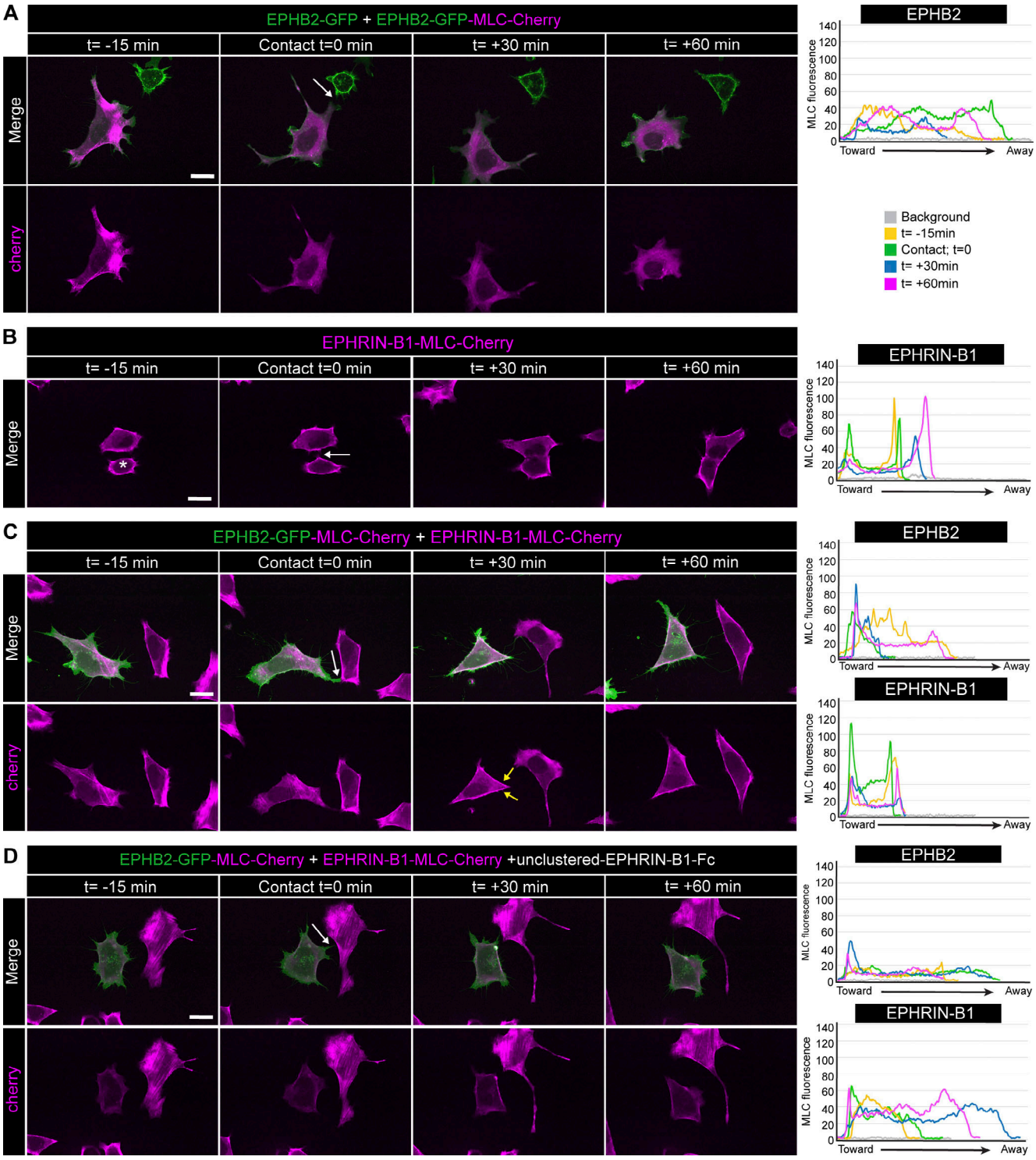

Figure S4. **MLC localization increases at heterotypic contacts. (A)** Example images from live imaging experiments (Video 9) of EPHB2 homotypic conditions at low density. EPHB2-GFP (green) cells were mixed with EPHB2-GFP-MLC-Cherry (magenta). Line scan analysis of the cell pair at various time points shows no change in MLC localization upon contact. **(B)** Example images from live imaging experiments (Video 10) of EPHRIN-B1 homotypic conditions at low density. EPHRIN-B1-MLC-Cherry (magenta). The asterisk indicates analyzed cell. Line scan analysis of the cell pair at various time points shows no change in MLC localization upon contact. **(C)** Example images from live imaging experiments (Video 11) of heterotypic conditions at low density. EPHB2-GFP-MLC-Cherry (green) cells were mixed with EPHRIN-B1-MLC-Cherry (magenta) cells. Yellow arrows at t = 30 min indicate localized increase in MLC. Line scan analysis of the cell pair at various time points shows that MLC localized to cell contact in EPHB2 cells upon contact. **(D)** Example images from live imaging experiments (Video 12) of heterotypic, with unclustered-EPHRIN-B1-Fc, conditions at low density. EPHB2-GFP-MLC-Cherry (green) cells were mixed with EPHRIN-B1-MLC-Cherry (magenta) cells; unclustered-EPHRIN-B1-Fc was added to prevent signaling. Line scan analysis of the cell pair at various time points shows no change in MLC localization upon contact. White arrow at t = 0 min indicates point of contact. Toward indicates toward contact, while away indicates away from contact. Scale bars, 20 µm.

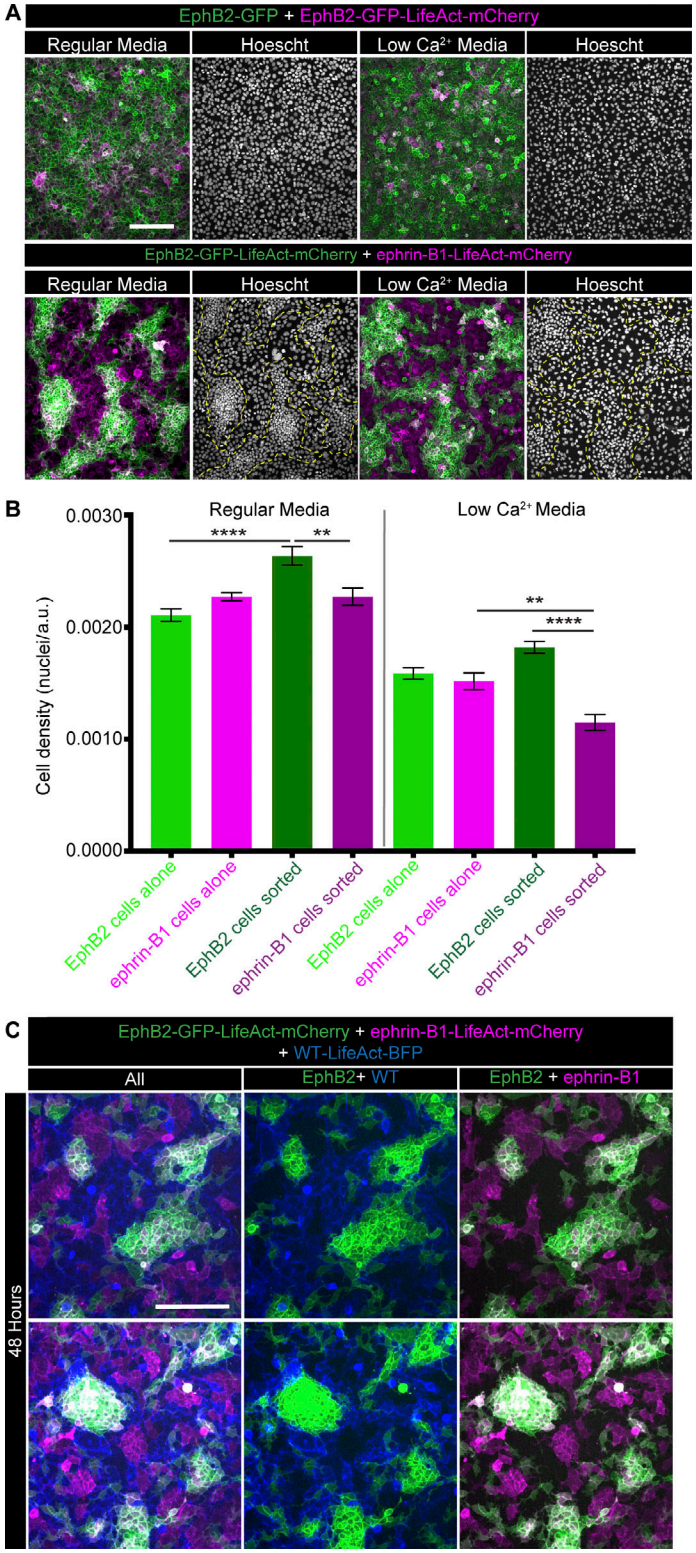

Figure S5. **EPHB2 cells increase homotypic contacts in response to EPH/EPHRIN signaling. (A)** Cell segregation in mixed populations of HEK293 cells at 48 h. In the left panels, EPHB2-GFP (green) cells were mixed with EPHB2-GFP-LifeAct-mCherry (magenta) cells in either regular or low-Ca^{2+} media. In the right panels, cells EPHB2-GFP-LifeAct-mCherry were mixed with cells overexpressing EPHRIN-B1-LifeAct-mCherry (magenta) in regular HEK293 or low-Ca^{2+} media. Hoescht images shown to visualize nuclei. Yellow dashed lines outline EPHB2 cell patches. Scale bar, 200 µm. **(B)** Quantification of nuclear density for the conditions illustrated in (A). In both regular and low-Ca^{2+} media, EPHB2 cells have a significantly increased density. Column heights represent means of the technical replicates, and error bars represent SEM. **, $P < 0.01$; ****, $P < 0.0001$. **(C)** Cell segregation in mixed populations of HEK293 cells. EPHB2-GFP (green) cells were mixed with EPHRIN-B1-LifeAct-mCherry (magenta) cells and WT-LifeAct-BFP (blue) cells. Cell segregation robustly occurs, and WT-LifeAct-BFP cells do not intermix with EPHB2 cells. Scale bar, 200 µm.

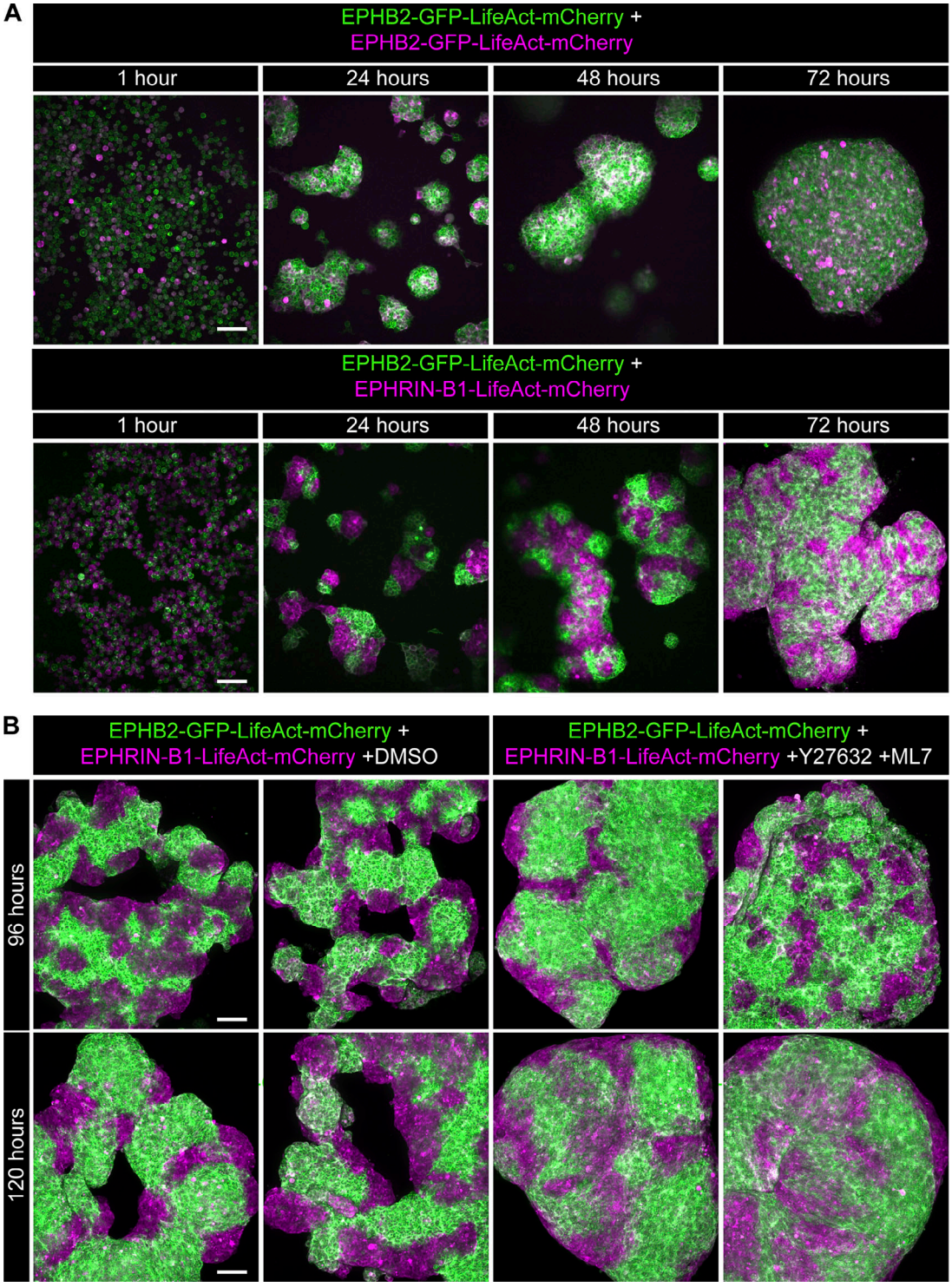

Figure S6. **EPH/EPHRIN signaling effects on cortical tension impact tissue morphology. (A)** Top: Representative images of EPHB2-GFP (green) cells mixed with EPHB2-GFP-LifeAct-mCherry (magenta) cells in hanging drop cultures at multiple time points during aggregate formation. Bottom: Representative images of EPHB2-GFP-LifeAct-mCherry (green) cells mixed with cells overexpressing EPHRIN-B1-LifeAct-mCherry (magenta) at multiple time points during aggregate formation. Aggregates fully formed by 72 h. Scale bars, 100 µm. **(B)** Hanging drop aggregates formed by EPH:EPHRIN mixed cultures at 96 and 120 h with the addition of DMSO (controls) or Y27632 and ML7. Morphology changes observed in segregated aggregates are disrupted by inhibition of ROCK and MLCK with Y27632 and ML7. Scale bars, 50 µm.

Video 1. **Cell:cell contact dynamics in EPHB2 homotypic cell pairs.** EPHB2-GFP-LifeAct-mCherry (green). Analyzed by time-lapse confocal microscopy using a cell observer spinning disk confocal microscope (Zeiss) every 5 min for 12 h. Scale bar, 10 µm. Playback speed, 3 frames per second.

Video 2. **Cell:cell contact dynamics in EPHB2:EPHRINB1 heterotypic cell pairs.** EPHB2-GFP-LifeAct-mCherry (green) and EPHRIN-B1-LifeAct-mCherry (magenta). Analyzed by time-lapse confocal microscopy using a cell observer spinning disk confocal microscope (Zeiss) every 5 min for 12 h. Scale bar, 10 µm. Playback speed, 3 frames per second.

Video 3. **Cell:cell contact dynamics in EPHB2:EPHRINB1 heterotypic cell pairs.** EPHB2-GFP-LifeAct-mCherry (green) and EPHRIN-B1-LifeAct-mCherry (magenta). Analyzed by time-lapse confocal microscopy using a cell observer spinning disk confocal microscope (Zeiss) every 5 min for 12 h. Scale bar, 10 µm. Playback speed, 3 frames per second.

Video 4. **Cell:cell contact dynamics in EPHRINB1 homotypic cell pairs.** EPHRIN-B1-LifeAct-mCherry (magenta). Analyzed by time-lapse confocal microscopy using a cell observer spinning disk confocal microscope (Zeiss) every 5 min for 12 h. Scale bar, 10 µm. Playback speed, 3 frames per second.

Video 5. **MLC localization upon cell:cell contact.** EPHB2-GFP (green) and EPHB2-GFP-MLC-Cherry (magenta) cells. Analyzed by time-lapse confocal microscopy using a cell observer spinning disk confocal microscope (Zeiss) every 3 min for 90 min. White arrow indicates contact at 0 min. Scale bar, 20 µm. Playback speed, 3 frames per second.

Video 6. **MLC localization upon cell:cell contact.** EPHRIN-B1-MLC-Cherry (magenta) cells. Analyzed by time-lapse confocal microscopy using a cell observer spinning disk confocal microscope (Zeiss) every 3 min for 90 min. White arrow indicates contact at 0 min. Scale bar, 20 µm. Playback speed, 3 frames per second.

Video 7. **MLC localization upon cell:cell contact.** EPHB2-GFP-MLC-Cherry (green) and EPHRIN-B1-MLC-mCherry (magenta) cells. Analyzed by time-lapse confocal microscopy using a cell observer spinning disk confocal microscope (Zeiss) every 3 min for 90 min. White arrow indicates contact at 0 min, and yellow arrows at 30 min indicate localized increase in MLC. Scale bar, 20 µm. Playback speed, 3 frames per second.

Video 8. **MLC localization upon cell:cell contact.** EPHB2-GFP-MLC-Cherry (green) and EPHRIN-B1-MLC-mCherry (magenta) cells with unclustered-EPHRIN-B1-Fc. Analyzed by time-lapse confocal microscopy using a cell observer spinning disk confocal microscope (Zeiss) every 3 min for 90 min. White arrow indicates contact at 0 min. Scale bar, 20 µm. Playback speed, 3 frames per second.

Video 9. **MLC localization upon cell:cell contact.** EPHB2-GFP (green) and EPHB2-GFP-MLC-Cherry (magenta) cells. Analyzed by time-lapse confocal microscopy using a cell observer spinning disk confocal microscope (Zeiss) every 3 min for 90 min. White arrow indicates contact at 0 min. Scale bar, 20 µm. Playback speed, 3 frames per second.

Video 10. **MLC localization upon cell:cell contact.** EPHRIN-B1-MLC-Cherry (magenta) cells. Analyzed by time-lapse confocal microscopy using a cell observer spinning disk confocal microscope (Zeiss) every 3 min for 90 min. White arrow indicates contact at 0 min. Scale bar, 20 µm. Playback speed, 3 frames per second.

Video 11. **MLC localization upon cell:cell contact.** EPHB2-GFP-MLC-Cherry (green) and EPHRIN-B1-MLC-Cherry (magenta) cells. Analyzed by time-lapse confocal microscopy using a cell observer spinning disk confocal microscope (Zeiss) every 3 min for 90 min. White arrow indicates contact at 0 min, and yellow arrows at 30 min indicate localized increase in MLC. Scale bar, 20 µm. Playback speed, 3 frames per second.

Video 12. **MLC localization upon cell:cell contact.** EPHB2-GFP-MLC-Cherry (green) and EPHRIN-B1-MLC-Cherry (magenta) cells with unclustered-EPHRIN-B1-Fc. Analyzed by time-lapse confocal microscopy using a cell observer spinning disk confocal microscope (Zeiss) every 3 min for 90 min. White arrow indicates contact at 0 min. Scale bar, 20 µm. Playback speed, 3 frames per second.

Table S1, Table S2, and Table S3 are provided online as separate Excel files. Table S1 lists the sample sizes and replicates. Table S2 lists the crosses used to generate experimental and control embryos. Table S3 lists the number of embryos analyzed.